JIMMA UNIVERSITY

JIMMA INSTITUTE OF TECHNOLOGY

FACULTY OF ELECTRICAL AND COMPUTER ENGINEERING

POST GRADUATE PROGRAM IN COMMUNICATION ENGINEERING

CHANNEL CAPACITY ANALYSIS FOR FBMC/OQAM BASED MASSIVE MIMO SYSTEMS

DIRIBA CHALI
ID.No. RM-1025/09

A thesis submitted to Faculty of Electrical and Computer Engineering in partial fulfilment of the requirements for the Master of Science degree in Communication Engineering.

July, 2019
Jimma, Ethiopia

JIMMA UNIVERSITY

JIMMA INSTITUTE OF TECHNOLOGY

FACULTY OF ELECTRICAL AND COMPUTER ENGINEERING

POST GRADUATE PROGRAM IN COMMUNICATION ENGINEERING

CHANNEL CAPACITY ANALYSIS FOR FBMC/OQAM BASED MASSIVE MIMO SYSTEMS

DIRIBA CHALI

Advisor Name: Kinde Anlay (PhD)

Co-advisor Name: Getachew Alemu(Msc)

A thesis submitted to Faculty of Electrical and Computer Engineering in partial fulfilment of the requirements for the Master of Science degree in Communication Engineering.

July, 2019

Jimma, Ethiopia

Declaration

This thesis is my original work and has not been presented for a Degree in any other Universities.

Thesis submitted by

Diriba Chali _____ _____

SIGNATURE DATE

APPROVED BY ADVISORS:

ADVISOR: _____ _____

SIGNATURE DATE

CO-ADVISOR: _____ _____-

SIGNATURE DATE

Approved by Faculty of Electrical and computer engineering research Examination members

1. _____ _____ _____

SIGNATURE DATE

2. _____ _____ _____

SIGNATURE DATE

3. _____ _____ _____

SIGNATURE DATE

Acknowledgments

It is a great honor to me in expresses my gratitude to all those people who have continuously supported me and had their contributions in making this thesis possible.

I would like to express my sincere thanks and appreciation to my advisor, Kinde Anlay (PhD), and my Co-advisor Getachew Alemu(MSc) for giving me constant trust during the entire research of my MSC thesis studies, for their helpful suggestions and advices, for their continuous support and their teachings essential to achieve this objective.

I also wish to thank all colleagues and technical staffs in Jimma Institute of Technology for their prompt support and helpful in providing all the facilities required for my research work.

Last but not least, I would like to acknowledge my family , for their constant love and encouragement.

Abstract

One characteristics of filter bank multicarrier offset quadrature amplitude modulation (FBMC/OQAM) is that the demodulated transmitted symbols are accompanied by interference terms caused by the neighboring transmitted data in time-frequency domain. The presence of this interference is an issue for some Massive MIMO systms and until today their combination with FBMC/OQAM remains an open problem.

In this thesis, a study on channel capacity of the massive multi-input multi-output (MIMO)system in the context of FBMC/OQAM and the effects of channel distortions has been carried-out. One advantage of FBMC to massive MIMO channels is self-equalization property. Due to this property, the effects of channel distortions will decrease by increasing the number of BS antennas, but,do not vanish as the base station (BS) array size increases in frequency selective channels. As a result, channel capacity cannot grow effectively by increasing the number of BS antennas. This is caused by the correlation between the multi-antenna combining tap values and the channel impulse responses between the mobile terminals and the BS antennas. To resolve this problem, a channel equalizer is introduced. This enabling us to achieve arbitrarily large SINR values by increasing the number of BS antennas and to improve channel capacity of the system.

This improvement is demonstrated through matlab software with selected numerical values of the basic parameters. As simulation result shows that, signal to interference plus noise ratio (SINR)value increased by 17dB per user for Minimum Mean-Square Error (MMSE)and zero forcing(ZF), and 2dB per user for maximum ratio combiners (MRC). Similarly, the achievable rate increases by 6 bits per second per hertz for ZF and MMSE, and 1 bits per second per hertz for MRC. Also, the throughput increased by 54 megabits per second for ZF and MMSE and and 8 megabits per second for MRC. Moreover, with the channel equalizer, it is not necessary to have a flat channel response over the band of each sub-carrier in order to use single-tap equalizer.

Keywords: Massive MIMO, FBMC/OQAM, SINR, channel equalizer, channel capacity, linear combiners, prototype filter.

Contents

List of Abbrevations

AFB	Analysis filter bank
AWGN	Additive white Gaussian noise
BER	Bit error rate
BS	Base station
CFO	Carrier frequency offset
CFR	Channel frequency response
CIR	Channel impulse response
CP	Cyclic prefix
CSI	Channel state information
DFT	Discrete Fourier transform
FBMC	Filter bank multicarrier
FOFDM	Filtered orthogonal frequency division multiplexing
FFT	Fast Fourier Transform
FIR	Finite impulse response
GFDM	Generalized frequency division multiplexing
ICI	Inter-carrier interference
IDFT	Inverse DFT
IFFT	Inverse FFT
IN	Interference plus noise
ISI	Inter-symbol interference
MRC	Maximum ratio combiner
MCM	Multicarrier modulation
MIMO	Multiple-input-multiple-output
MMSE	Minimum mean square error
OFDM	Orthogonal frequency division multiplexing
OQAM	Offset quadrature amplitude modulation
PAPR	Peak-to-Average Power Ratio
PDP	power delay profile
PPN	Polyphase network
PHYDYAS	PHYsical layer for DYnamic spectrum AccesS and cognitive radio

QAM	Quadrature amplitude modulation
SFB	Synthesis filter bank
SINR	Signal to interference plus noise ratio
SISO	Single-input-single-output
SNR	Signal to noise ratio
S/P	Serial to parallel
TMUX	Transmultiplexer
TO	Time offset
Tx	Transmitter
UFMC	universal filtered multicarrier
UMTS	Universal Mobile Telecommunications System
WiMAX	Worldwide Interoperability for Microwave Access
WOFDM	Windowed orthogonal frequency division multiplexing
ZF	Zero forcing

List of Figures

Chapter 1

Introduction

1.1 Background

The early digital communication systems were centered on single carrier modulation scheme. Generally, if we want to increase the transmission system bit rate, we have to minimize the symbol duration. However, the existence of a multipath channel presents inter-symbol interference (ISI) which needs complex equalization. Multi-carrier modulations have been then presented as a good alternative in order to counteract the effects of multi-path fading. Indeed, in multi-carrier communications data is transmitted over many frequencies instead of a single carrier, dividing the wide-band frequency selective communication channel into various sub-bands with mildly selective fading.

Orthogonal Frequency Division Multiplexing (OFDM) is the most common multicarrier modulation scheme. It has been considered as essential part in various wireless communication systems such as WiFi based on the IEEE 802.11 standard, WiMax (Worldwide Interoperability for Microwave Access) based on the IEEE 802.16 standard, Long Term Evolution (LTE), LTE-advanced, ... etc[[2]- [5]]. It offers many attractive advantages such as efficient hardware implementation, low complexity equalization, and compatibility with multiple-input multi-output (MIMO) technologies. Also, it has high spectral efficiency using closely spaced orthogonal subcarriers and robustness to multipath fading effects. Moreover, it has ability to avoid both ISI and ICI by appending a cyclic prefix (CP) that significantly reduces the complexity of the equalization to a single complex coefficient per subcarrier equalizer. It is used in the massive MIMO to improve capacity of

current wireless because it is simple and robust to against multipath channels [7]. However, OFDM suffers from a large spectral leakage leading to high out-of-band emissions due to the high side-lobe levels of the subcarriers. Also, in the uplink of multiuser networks, stringent synchronization procedures are required. The users may experience different doppler shifts, frequency offsets, timing offsets, etc., and to maintain the orthogonality between the subcarriers, energy and resource are needed. Due to high side-lobe levels of its subcarriers, it is very difficult to utilize non-contiguous spectrum chunks through carrier aggregation for the future high data rate applications in the uplink with OFDM [10].

All these disadvantages avoid the OFDM adoption in the 5G air interface to attain the following important characteristics presently intended for 5G wireless networks [24]:

- 1000 times higher mobile data volume per geographical area
- 10 - 100 times more connected devices
- 10 - 100 times higher typical user data rate
- 10 times lower energy consumption
- End-to-end latency of $< 1ms$
- Ubiquitous 5G access including in low density areas

Therefore, considering the above-mentioned OFDM disadvantages and the wireless networks new requirements, a great deal of interest in the area of waveform design has been emerged. These began among the research and industrial communities motivating introduction of alternative wave-forms capable of keeping the advantages of OFDM while addressing its disadvantages. The waveforms presently under assumtion include filtered orthogonal frequency division multiplexing (FOFDM) [26], windowed orthogonal frequency division multiplexing (WOFDM) [27], filterbank multicarrier (FBMC) [28], generalized frequency division multiplexing (GFDM) [29] and universal filtered multicarrier (UFMC) [25]. The FBMC appears to be a good candidate for 5G systems between these multiple access methods. It is a multicarrier modulation(MCM) techniques that offering significantly improved spectral properties over OFDM by shaping the subcarriers using a prototype filter. This prototype filter is well localized in both time and frequency. Therefore, the uplink synchronization requirements can be substantially

relaxed, and carrier aggregation becomes a trivial task [18]. Also it offers several advantages such as lower spectral leakage and reduced sensitivity to doppler effects [15, 16]. It exhibits better spectrum shape compared to OFDM and enables better spectrum usage and improved mobility support [17].

To fulfill the expectations of 5g, the combination of FBMC/OQAM and massive MIMO systems have received a lot of attention in the wireless communication [6]. So, Massive MIMO has been considered as a promising technology for next generation wireless systems and it addresses significant challenges in 5G [8, 9]. It is a system in which transmitter uses large number of antennas about hundred or more and serving many users simultaneously in the same time frequency resource [10]. The combination of FBMC-OQAM modulations with massive MIMO communications was first studied in [18]. This combination gives self-equalization property that leads a channel flattening effect. But, due to the generation of inter-symbol interference (ISI) and inter-carrier interference (ICI), the orthogonality of FBMC-OQAM between subcarriers is progressively destroyed as the channel frequency selectivity becomes large in normal FBMC-OQAM, i.e., when the channel cannot be approximated as flat at the subcarrier level.

However, in massive MIMO, this interference decreases as the number of BS antennas increases, even in the case of strong channel selectivity for simple single-tap per-subcarrier receivers. This shows that a distortion floor is there even if the number of BS antennas grows without bounds, meaning that ICI and ISI are not completely removed. As a result, the signal-to-interference-plus-noise ratio (SINR) cannot grow unboundedly by increasing the number of BS antennas, and is upper bounded by a certain deterministic value. This phenomenon is a result of the correlation between the multi-antenna combining tap values and the channel impulse responses between the mobile terminals and the BS antennas. To resolve this problem, a prototype and an efficient equalization method are used to remove this correlation, enabling us to achieve arbitrarily large SINR values by increasing the number of BS antennas [22, 23].

Due to this correlation between the multi-antenna combining tap values and the channel impulse responses between the mobile terminals and the BS antennas, channel capacity cannot increase efficiently by increasing the number of BS antennas. To increase channel capacity of the FBMC-OQAM Massive MIMO channel

by increasing the number of BS antennas, a channel equalizers are used to removes this correlation. So, in this thesis channel capacity or performance of the FBMC-OQAM Massive MIMO channel is analyzed in terms of bit error rate, throughput, achievable rate/spectral efficiency, system complexity and the signal-to-interference-plus-noise ratio (SINR)using matlab simulation and the result is shown in chapter five. The focus of this study is on the uplink transmission and it is applicable for downlink transmission. Single-tap equalization per subcarrier is considered, and the performance of two most prominent linear combiners, namely, maximum-ratio combining (MRC), zero-forcing (ZF) and Minimum Mean-Square Error (MMSE) have investigated.

1.2 Statement of the problem

One of the advantage of the FBMC in the massive MIMO channels is that self-equalization effect, the subcarrier spacing can be increased in massive MIMO FBMC systems, reducing the number of subcarriers and leading to a lower sensitivity to carrier frequency offset and peak-to average- power-ratio. In the SISO, the FBMC-OQAM orthogonality is well known to be progressively destroyed as the channel frequency selectivity becomes large, i.e., when the channel cannot be approximated as flat at the subcarrier level. This is due to the generation of inter-symbol interference (ISI) and intercarrier interference (ICI). However, in massive MIMO, it appears that this interference decreases as the number of BS antennas increases, even in the case of strong channel selectivity. This shows that a distortion floor is there even if the number of BS antennas grow without bounds, meaning that ICI and ISI are not completely removed. As a result, the signal-to-interference-plus-noise ratio (SINR)and channel capacity cannot grow effectively by increasing the number of BS antennas. This phenomenon is a result of the correlation between the multi-antenna combining tap values and the channel impulse responses between the mobile terminals and the BS antennas.

1.3 Objectives of the research

The general objective of this thesis is to analyze the performance of channel capacity for Filter Bank Multicarrier Massive MIMO based on Channel Equalizer.

1.3.1 Specific objectives

The specific objectives of this study are the following:

- to derive the SINR for FBMC massive MIMO without channel equalizer and with channel equalizer using MRC, ZF, and MMSE combiners.
- to evaluate the sum rate/achievable rate for FBMC massive MIMO without channel equalizer and with channel equalizer using ZF, MMSE and MRC linear combiners.
- to analyze the complexity of the FBMC system without channel equalizer and with channel equalizer.
- to analyze the spectral efficiency and the throughput of the FBMC Massive MIMO systems without channel equalizer and with channel equalizer.
- to find the bit error rate (BER)for FBMC Massive MIMO with channel equalizer and without channel equalizer.

1.4 Contributions

The main contributions in this work are related to addressing some of the key challenges in FBMC/OQAM Massive MIMO systems and channel capacity analysis of Massive MIMO-FBMC system. The key challenge in this system is, there is a correlation between the multi-antenna combining tap values and the channel impulse responses between the mobile terminals and the BS antennas. This may limit the channel capacity of the system. To avoid this, the channel equalizer is used in Massive MIMO-FBMC system. The main work in this contribution is summarized as follows:

- to analyze the channel capacity with and without channel equalizer by increasing the BS array size.
- A mathematical model of Massive MIMO-FBMC/OQAM system with channel equalizer effect on the detection performance in terms of the SINR and achievable rate using MRC, ZF and MMSE combiners by comparing with that of the conventional Massive MIMO-FBMC/OQAM system have analyzed.

- to evaluate FBMC system computational complexity with and without channel equalizer.
- Based on the mathematical model, also then the impact of channel equalizer on the system performance analyzed through simulation results.

1.5 Thesis Organization

Chapter 2 provides a literary overview of the several topics and concepts that will be covered over the course of this thesis. It contains an introduction to transmultiplexers and FBMC systems with Massive MIMO systems. Chapter 3 presents candidate waveform for 5G and the FBMC/OQAM transmultiplexer models that deals with the polyphase implementation. A very brief overview of comparison of candidate waveforms and prototype filters are provided. Then, the fundamental theory of FBMC-OQAM system is given with much emphasis on transmitter and receiver side. In that aspects such as the OQAM mapping, polyphase filtering, discrete-time representation, FBMC-OQAM modulation, prototype filtering, orthogonality and overlapping nature have been discussed. Chapter 4 We introduced the principle of FBMC/OQAM modulation technique along with the prototype filters use in this scheme. We then discuss the combination of FBMC system with technique like Massive MIMO which introduces the analysis and implementation of FBMC/OQAM Massive MIMO System. It discusses the design and its channel equalization implementation in detail, and the performance of the system. Chapter 5 and 6 draws final conclusions of the thesis, briefly summarizes the main obtained results, and possible future research directions.

Chapter 2

Literature Review

Recently, massive MIMO has been proposed to further maximize network capacity and to conserve energy and interest in the field of wireless communications due to their ability to increase data throughput and improve link quality. How it maximize network capacity is, the base station (BS) is equipped with a large number of antenna elements, in the order of hundreds or more, and is simultaneously serving tens of mobile terminals (MTs) [9] and the effects of uncorrelated noise and multiuser interference can be made arbitrarily small as the BS array size increases by coherent processing of the signals over the BS antennas [8].

Orthogonal frequency division multiplexing (OFDM) is a multi-carrier modulation technique with immunity to the channels frequency selectivity, which can transmit data over large numbers of sub-carriers rather than a single carrier transmission. It considered in the Massive MIMO because of its simplicity and robustness against multipath channels [7]. However, OFDM suffers from a large spectral leakage leading to high out-of-band emissions due to the high side-lobe levels of the subcarriers. and stringent synchronization are required in the uplink of multiuser networks. Due to the high side-lobe levels of the subcarriers, it very difficult to utilize non-contiguous spectrum chunks through carrier aggregation for the future high data rate applications in the uplink with OFDM [10]. Moreover, to avoid interference, large guard bands are required between adjacent frequency channels, which in turn, lower the spectral efficiency of OFDM it uses cyclic prefix. A cyclic prefix used in OFDM reduces the throughput of the transmission and also wastes power. It is sensitive to Doppler shifts, carrier frequency offsets, timing offsets, etc., and to maintain the orthogonality between the sub-carriers, it needs additional energy and resource for synchronization procedures. Additionally, its signal

has a noise like amplitude with a very large dynamic range; therefore it requires RF power amplifiers with a high peak to average power ratio.

To overcome the drawbacks of OFDM and to fulfill a vast variety of requirements and applications of the next generations of wireless networks, researcher and industrial communities has been designed new waveforms, keeping the advantages of OFDM while addressing its drawbacks [12, 13, 14]. For instance, recently, the standardization bodies have laid down the foundation of the fifth generation of wireless networks (5G) by defining its primary objectives [20]. New applications like enhanced mobile broadband (eMBB), massive machine-type communications (mMTC), and ultra-reliable low-latency communications (URLLC) are anticipated in 5G. These new applications require high data rate, number of connected devices, good spectrum efficiency, high battery life, and low end-to-end latency as compared to the current wireless and wired communications, [11].

Filter bank multicarrier (FBMC) is a multi-carrier modulation techniques or a waveform that is development of OFDM and aims to overcome the drawbacks of OFDM. It offers significantly improved spectral properties over OFDM by shaping the subcarriers using a prototype filter that is well localized in both time and frequency [15]. Also, because of the very low out-of-band emission of subcarrier filters, application of FBMC in the uplink of multiuser networks is trivial. Also, it can be deployed without synchronization of mobile user nodes signals. In the application of cognitive radios, the filter bank that is used for multicarrier data transmission can also be used for spectrum sensing [16, 17].

Moreover, this FBMC can combine with the Massive MIMO sytems easly to improve the performance of communication systems using a single-tap equalization and multi-tap equalization per subcarrier. For FBMC-based massive MIMO systems, the proposed multi-tap equalization per subcarrier improves the equalization accuracy as compared to the with the expense of a higher computational complexity [19]. In the multi-cellular massive MIMO networks, pilot contamination problem is occurred [7]. This problem can be resolved in a straightforward manner with FBMC signaling due to its special structure [21]. That means FBMC is a proper match for massive MIMO and vice versa as they can both bring pivotal properties into the picture of the next generations of wireless systems. The combination of FBMC-OQAM and massive MIMO gives some applications and many advantages over normal FBMC-OQAM. Self-equalization property is one of the applications

of FBMC and massive MIMO channels combinations, has been recently studied in [18]. Due to a channel flattening effect obtained in this application, the effects of channel distortions (i.e., inter-symbol interference and inter-carrier interference) will diminish by increasing the number of BS antennas. This combination not only great importance as the same spectrum is being simultaneously utilized by all the users but it is also used in a more efficient manner compared to OFDM.

In the combination of FBMC-OQAM and massive MIMO, the effects of channel distortions (i.e., inter-symbol interference and inter-carrier interference) will diminish by increasing the number of BS antennas. This shown that a distortion floor remains even if the number of BS antennas grows without bounds, meaning that ICI and ISI are not completely removed. As a result, the signal-to-interference-plus-noise ratio (SINR) cannot grow unboundedly by increasing the number of BS antennas, and is upper bounded by a certain deterministic value. This phenomenon is a result of the correlation between the multi-antenna combining tap values and the channel impulse responses between the mobile terminals and the BS antennas. To resolve this problem, a prototype and an efficient equalization method are used to removes this correlation, enabling us to achieve arbitrarily large SINR values by increasing the number of BS antennas [22, 23].

However,the performance analysis of the massive MIMO FBMC/OQAM system is achieved by these researches using linear combiners, namely MRC and ZF only. Additionally, the effect of the correlation on channel capacity is not done directly. Also, the analysis of complexity reduction as the effect of channel equalizer is not presented in detail.

Therefore, the channel capacity cannot increases highly by increasing the number of BS antennas due to the correlation effect. To increase channel capacity of the FBMC-OQAM Massive MIMO channel with increasing the number of BS antennas, the channel equalizer is used to removes this correlation. So in this thesis channel capacity or performance of the Massive MIMO FBMC-OQAM systems are analyzed in terms of bit error rate(BER), throughput, spectral efficiency and system complexity with and without channel equalizer. A Single-tap equalization per subcarrier will be considered, and the performance of three most prominent linear combiners, namely, maximum-ratio combining (MRC), Minimum Mean-Square Error (MMSE) and zero-forcing (ZF)have investigated.

Chapter 3

FBMC/OQAM system model

A wave-form that uses a square window in time domain permitting a very efficient implementation, Orthogonal frequency division multiplexing (OFDM)has been accepted as the air interface in various wireless communication standards such as long-term evolution (LTE), IEEE 802.11 standard families and third generation partnership (3GPP)due to the related advantages such as:

- efficient hardware implementation and low complexity equalization
- robustness to multipath fading effects
- Ease of implementation
- By using of cyclic prefix (CP), efficient one-tap frequency domain equalization is enabled.
- Simple extension and straightforward to very large MIMO and high gain beam forming solutions [24].

In spite of its advantages, OFDM Undergoes from a number of drawbacks such as high side lobes in frequency and high peak-to-average power ratio (PAPR). OFDM needs stringent time synchronization to preserve the orthogonality between various user equipments (UEs). Therefore, signaling overhead grows with the UEs number in an OFDM-based system. Moreover, it has high sensitivity to carrier frequency offset (CFO) mismatch between different devices. All these disadvantage avoid the OFDM adoption in the 5G air interface and attentiveness in the new waveform design area to achieve the requirements currently intended for wireless networks of 5G [24].

3.1 Candidate waveforms

Therefore, since the aforementioned OFDM drawbacks and the wireless networks new requirements, a great deal of concern in the waveform design area has been developed among the industrial communities and research motivating alternative waveform introduction keeping the advantages of OFDM capable while addressing its disadvantages, [6][10]. The different scenarios requirements can be affected by the waveforms choice. Therefore, the various physical-layer waveforms are being developed for 5G networks to address the disadvantage of OFDM and enable the aforementioned requirements. The waveforms presently under concern include windowed orthogonal frequency division multiplexing (WOFDM) [27], filtered orthogonal frequency division multiplexing (FOFDM) [26], generalized frequency division multiplexing (GFDM) [29], universal filtered multicarrier (UFMC) [25] and filterbank multicarrier (FBMC) [28].

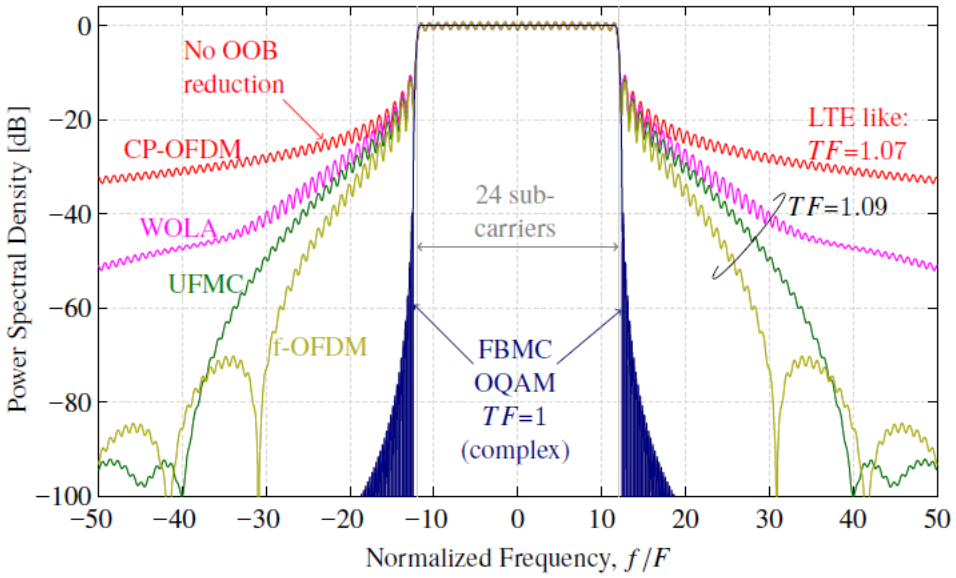

FIGURE 3.1: Different modulation techniques power spectral density

From Fig. 3.1 compared to CP-OFDM, FBMC has much improved spectral properties. Windowing (WOLA) and filtering (UFMC, f-OFDM) can improve the spectral properties of CP-OFDM. However, FBMC has the additional maximum symbol density, TF = 1 (complex) advantage and still implements much better others.

3.2 Filter bank multicarrier (FBMC)

The filter bank based multicarrier (FBMC) discards the CP to improve flexibility of the system and it introduces filter banks to the OFDM system to deal with some disadvantages of OFDM. To fulfill the requirements of communication system, such as to minimize the sideband power loss and improve the spectral efficiency, the filter bank can be designed with various properties. Since subcarrier filters require long filter lengths (normally at least 4T to preserve an acceptable ISI and ICI) becuase they are narrow in frequency and in time the symbols are overlapping. In QAM, data can be transitted randomly such that 00 can be followed by 11 (there is a diagonal transition) from constellation diagram for 4-QAM, which several changes in the amplitude. These large change in the amplitude causes large out of band emission. To prevent these transitions, offset QAM is introdued where one allow only 90 degrees phase shift which accomplished by delaying ethier of the Q or I channel by half symbol time period. Moreover, FBMC obeys the real orthogonality condition by applying offset-QAM (OQAM) and, therefore, it is not orthogonal in the complex domain. And, it is known as OFDM with offset QAM (OFDM/OQAM) and the most common FBMC technique is the FBMC/OQAM [31].

The filter bank multicarrier (FBMC)techniques that based on Offset quadrature amplitude modulation utilize filter-bank which is depend on trans-multiplexers in order to channelize the band of wide signal. The filter banks that contains synthesis and analysis filters are typically developed from a prototype filter that decides the performance of system, including inter-carrier interference(ICI)and inter-symbol interference (ISI), and stop-band attenuation. To eliminate ISI and ICI, and keep the side lobes small, the prototype filter needs to be carefully designed. There are two types of FBMC implementations such as the frequency spreading filter bank multicarrier (FS-FBMC) and the poly-phase network filter bank multi-carrier (PPN-FBMC) in order to simplify the filter design.

The PPN-FBMC is selected as the model in this thesis in order to reduce the high complexity which is introduced by the extra filtering operations at the transmitter and receiver. The PPN FBMC transceiver system basic block diagram is shown in Figure 3.2. The prototype filters are implemented using polyphase implementation, that uses multi-rate signal processing techniques to reduce the complexity by combined implementation of all analysis or synthesis filters in the filter bank. The transmitted signal is the sum of a M filters bank the outputs in the FBMC,

with filter length $L = M \times O$, where M is the FFT size and O is the prototype filter overlapping factor. A PHYDYAS prototype function with O = 4, for use in FBMC system, which is well-localized in time and frequency domain is used in this paper. Since due to more advanced prototype filter design, sub-carriers

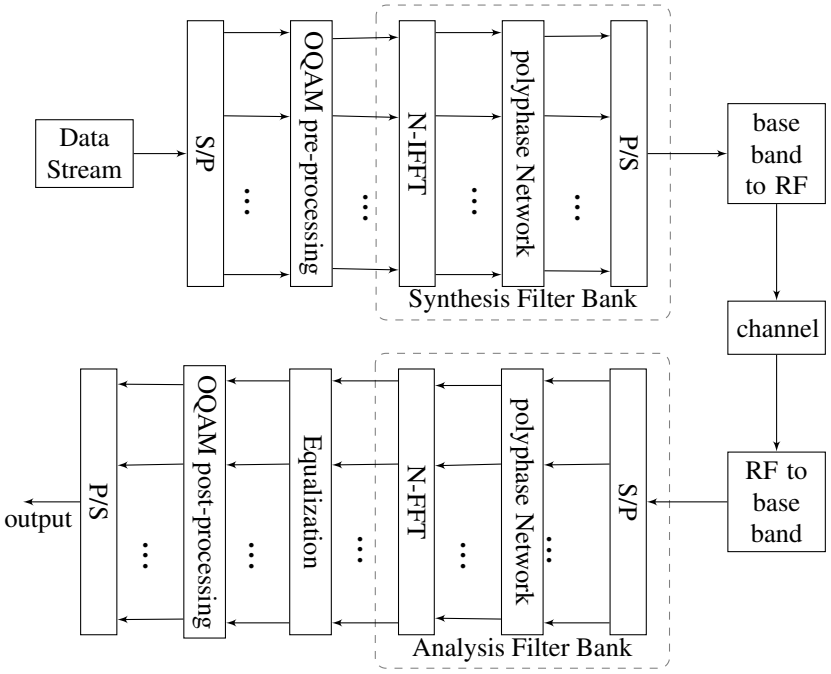

FIGURE 3.2: FBMC/OQAM system model

can be better localized in FBMC and the CP can be detached resulting in increased spectral efficiency when it compared to OFDM. Moreover, due to reduced guard band in the FBMC, good the spectral efficiency gain is obtained. However, FBMC/OQAM suffers an overhead becuase of transition times (tails), which its duration is equal to the prototype filter length, a transmission burst at both ends and an overhead becuase of the T=2 time offset between the OQAM symbols [32]. Without increasing its sensitivity to time and frequency misalignmen, the overhead cannot be avoided totally, and it growths the communication latency, but, to reduce OFDM/OQAM signals tails of signal the solutions have been proposed in [32].

The FBMC system in Figure 3.2 is simplified using trans-multiplexer configurations as shown in Figure 3.3. The main processing blocks of FBMC system in direct form representation are OQAM pre-processing, synthesis filter bank, analysis filter bank, and OQAM post-processing. The transmission channel is typically not included during TMUX systems designing and analyzing since handling the channel equalization problem is done separately.

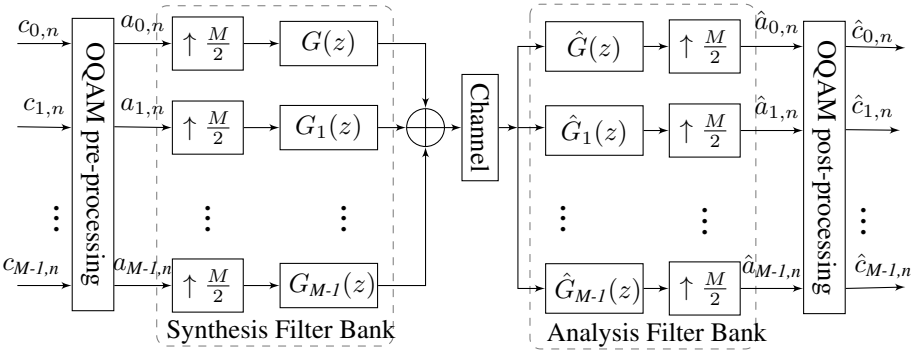

FIGURE 3.3: Transmultiplexer configurations.

3.2.1 OQAM mapping

it is possible to attain a baud-rate spacing among adjacent subcarrier channels by introducing a half symbol period shift between the in-phase and quadrature QAM symbols components,while recovering the information symbols without ISI and ICI is still possible [33]. So, an OQAM modulates each subcarrier and the orthogonality principles are well-thought-out only in the real field [28]. In order to keep neighboring carriers orthogonality condition in OQAM mapping, pure imaginary and real values alternate on successive transmitted symbols and successive carrier frequencies for a specified carrier at the transmitter side (3.1).

OQAM pre/post-processing

Figure 3.4 is the pre-processing block that employs the transformation from QAM symbols to OQAM symbols. The input complex symbols values $c_{k,n}$ are changed to real symbols, where $k = 0, 1, ..., M-1$ and $n = 0, 1, ..., N^{'}-1$ are sub-carrier index and symbol index, respectively, in OQAM pre-processing (C2R) blocks. $c_{k,n}$ real and imaginary parts are upsampled by a 2 factor so that:(3.2)

$$c_{k,n}^{R} = \begin{cases} \Re\{c_{k,\frac{n}{2}}\}, & n \ even \\ 0, & elsewhere \end{cases} \tag{3.1}$$

and

$$c_{k,n}^{I} = \begin{cases} \Im\{c_{k,\frac{n}{2}}\}, & n \ even \\ 0, & elsewhere \end{cases} \tag{3.2}$$

Then, $c^I_{k,n}$ is delayed by one unit and is joined with the real values samples to finish OQAM pre-processing as, (3.3)

$$a_{k,n} = \phi_{k,n}\{c^R_{k,n} + c^I_{k,n}\} = a^R_{k,n} + a^I_{k,n}; \tag{3.3}$$

where in $n = 0, 1, ..., 2N^{'} - 1$ and $\phi_{k,n} = e^{j\pi(k+n)} = j^{(k+n)}$
For $0 \leq n^{'} \leq 2N^{'} - 1$, the complex input symbol vectors $\{C_{k,n}\}_{n=0}^{N^{'}-1}$ the OQAM mapping into real symbol $\{a_{k,n'}\}_{n'=0}^{2N^{'}-1}$ is done as shown below in(3.4)

$$\begin{aligned}
a_{k,n'} &= \begin{cases} c^R_{k,\lfloor\frac{n'}{2}\rfloor}, & n^{'}\, is\, even,\, k\, is\, even \\ c^I_{k,\lfloor\frac{n'}{2}\rfloor}, & n^{'}\, is\, odd,\, k\, is\, even \\ c^I_{k,\lfloor\frac{n'}{2}\rfloor}, & n^{'}\, is\, even,\, k\, is\, odd \\ c^R_{k,\lfloor\frac{n'}{2}\rfloor}, & n^{'}\, is\, odd,\, k\, is\, odd \end{cases} \\
&= \begin{cases} (1-\delta)c^R_{k,\lfloor\frac{n'}{2}\rfloor} + j\delta.c^I_{k,\lfloor\frac{n'}{2}\rfloor}, & n^{'}\, is\, even, \\ (1-\delta)c^I_{k,\lfloor\frac{n'}{2}\rfloor} + j\delta.c^R_{k,\lfloor\frac{n'}{2}\rfloor}, & n^{'}\, is\, odd, \end{cases} \\
&= [(1-\delta)(1-\theta) + \delta\theta].c^R_{k,\lfloor\frac{n'}{2}\rfloor} + [(1-\delta)\theta + \delta(1-\theta)].c^I_{k,\lfloor\frac{n'}{2}\rfloor}
\end{aligned} \tag{3.4}$$

where, $\theta = n^{'}\, modulo\, 2$ and $\delta = k\, modulo\, 2$. e.g. $a_{0,0} = c^R_{0,0}$, $a_{1,0} = c^I_{1,0}$, $a_{0,1} = c^I_{0,0}$ and $a_{1,1} = c^R_{10}$. The symbol period T is reduced to half in order to maximize the OQAM modulation spectral efficiency. Thus, the data received at the receiver side, may carries the real (or imaginary) signal components, and the imaginary (or real) parts seem as interference terms. For two consecutive sub-carrier, T/2 time-offset is presented onto the real part for the first sub-carrier and the imaginary part for the second one, therefore $N^{'}$ has to be even.

In the post-processing of the OQAM system, there are two somewhat different structures based on the sub-channel number as shown in Figure 3.5. The first one is the multiplication by $\phi^*_{k,n}$ sequence which is followed by the taking the real part operation. The second process is real-to-complex transformation, in which two consecutive real-valued symbols form a complex-valued symbol $\hat{c}_{k,n}$ and this operation is called as de-staggering. The real-to-complex transformation drops the sample rate by a two factor.

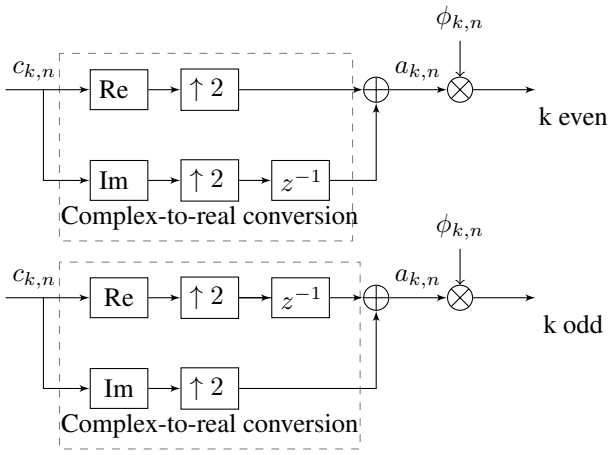

FIGURE 3.4: OQAM pre-processing.

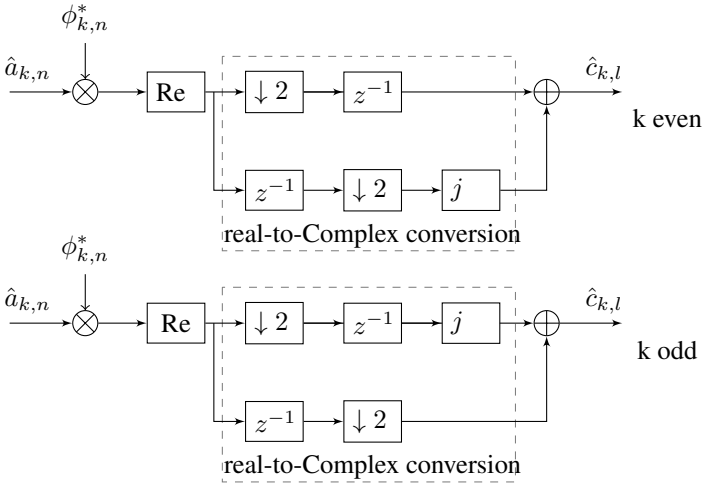

FIGURE 3.5: OQAM post-processing.

3.2.1.1 Synthesis and analysis filter banks

At transmitter side, the symbols $a_{k,n}$ are up-sampled by M/2 and up-sampled signals are then filtered with their analogous filter $G_k[z]$ to give M sub-channels in the SFB block. All sub-signals are added together and form the SFB output signal at the transmitter end. All sub-sub-carrier filters are created from a low pass prototype filter $g(m)$ with single real-valued linear-phase by using exponential modulation in the case complex modulated filter banks class is chosen. Hence, the resulting sub-channel filters are complex-valued due to the modulation function and therefore the advantageous frequency band is $[-\pi, \pi]$. Normally, two different channel types assembling preparations can be considered, namely, even-stacked filter banks and odd-stacked filter banks [34], [35]. The k^{th} sub-channel filters

center frequencies are $\omega_k = \frac{2k\pi}{M}$ and $\omega_k = \frac{(2k+1)\pi}{M}$ for even stacked and odd-stacked filter banks, respectively. The k^{th} synthesis filter is given by,(3.5)

$$g_k[m] = g[m]e^{\left(j\frac{2\pi k}{M}\left(m-\frac{L_p-1}{2}\right)\right)} \tag{3.5}$$

where $m = 0, 1, ..., L_p - 1$ and L_p is the filter length. It is considered that the prototype filter is intended in such a manner that there is no want for the extra scaling factor in order to simplify representations. The k^{th} analysis filter is easily a time-inverted and it is the corresponding synthesis filter complex-conjugated version as it given in (3.6)

$$\begin{aligned} f_k[m] &= g_k^*[L_p - 1 - m] \\ &= g[L_p - 1 - m]e^{\left(-j\frac{2\pi k}{M}\left(L_p-1-m-\frac{L_p-1}{2}\right)\right)} \\ &= g[m]e^{\left(j\frac{2\pi k}{M}\left(m-\frac{L_p-1}{2}\right)\right)} \end{aligned} \tag{3.6}$$

3.2.2 Polyphase Implementation

The direct form implementations of Figure 3.3 are not well-organized for practical applications because filtering operations are done at the high sampling rate prominent to a large number of unwanted calculations. Opportunely, there are different efficient multirate structures that are for needed for the filter banks such as lattice structures, polyphase structures and lapped transforms [36] [37]. The polyphase structures are the only ones that can be applied to Nearly perfect reconstruction (NPR) filter banks. Their main improvement is that they can give drastic oversimplifications because filtering operations are done at the lower sampling rate and wanted calculations are done. The FBMC/OQAM system efficient digitalimplementation is done through polyphase structures and DFT was first presented by Bellanger [38], and advanced and studied by Hirosaki [39].

3.2.2.1 Polyphase structure of synthesis filter bank

The synthesis filter bank has M sub-carriers with frequency spacing between them is Δf, which resulting in a signal bandwidth $B_w = M\Delta f$. The sampling interval T_s equals the signal bandwidth inverse ($T_s = 1/B_w = T/M$), according to the sampling theorem. The symbol period length is T, so the corresponding signal samples number is $T/T_s = M$ within each symbol period. By sampling the

continuous-time prototype filter $g(t)$, the discrete-time prototype filter is obtained within a sampling rate of T_s, which resulting in (3.7)

$$g[m] = g(mT_s), m = 0, 1, ..., L-1 \tag{3.7}$$

where L is the discrete-time prototype filter $g_T[m]$ length and the prototype filter length can be possible that larger than the symbol period. The prototype filter length is O times the symbol period,which is $L = OM$ assuming that O is the overlapping factor.

The discrete-time signal is converted into a complex frequency domain by using the Z-transform,which is an important analysis tool in communication syste. The $g_T[m]$ Z-transform is determined by (3.10)

$$G[z] = \sum_{m=0}^{L-1} g(m)z^{-m} = \sum_{m=0}^{ON-1} g(m)z^{-m} \tag{3.8}$$

Letting $m = l^{'}M + k^{'}$, where $l^{'} = 0, 1, ..., (O-1)$ and $k^{'} = 0, 1, ..., (M-1)$, Eq. (3.10) can be further converted into

$$\begin{aligned} G[z] &= \sum_{k^{'}=0}^{M-1} \sum_{l^{'}=0}^{O} g(l^{'}M + k^{'})z^{-(l^{'}M+k^{'})} \\ &= \sum_{k^{'}=0}^{M-1} z^{-k^{'}} \sum_{l^{'}=0}^{O} g(l^{'}M + k^{'})z^{-l^{'}M} \\ &= \sum_{k^{'}=0}^{M-1} G^{k^{'}}(z^M)z^{-k^{'}} \end{aligned} \tag{3.9}$$

Where $G^{k^{'}}(z^M)$ is polyphase filters,which is expressed as

$$G^{k^{'}}(z^M) = \sum_{l^{'}=0}^{O} g_T(l^{'}M + k^{'})z^{-l^{'}M} \tag{3.10}$$

The poly-phase filter number branches depends on the modulation function periodicity in the modulated filter banks. The modulation function periodicity used in Eqs.(3.5) and (3.6), i.e.,

$$\begin{aligned} e_k[m] &= e^{\left(j\frac{2\pi k}{M}\left(m-\frac{L_p-1}{2}\right)\right)} \\ &= e^{\left(-j\frac{2\pi k}{M}\left(\frac{L_p-1}{2}\right)\right)} e^{\left(j\frac{2\pi km}{M}\right)} \\ &= \beta_k e^{\left(j\frac{2\pi km}{M}\right)} \end{aligned} \tag{3.11}$$

Then in the poly-phase filters form, the k^{th} synthesis filter can be defined in as follows

$$\begin{aligned} G_k[z] &= \sum_{m=0}^{L-1} g(m) e_k[m] z^{-m} \\ &= \sum_{k'=0}^{M-1} \sum_{l'=0}^{O} g_m(l'M+k')\beta_k e^{\left(j\frac{2\pi k(l'M+k')}{M}\right)} z^{-(l'M+k')} \\ &= \sum_{k'=0}^{M-1} \beta_k e^{\left(j\frac{2\pi k'k}{M}\right)} z^{-k'} \sum_{l'=0}^{O} g(l'M+k') z^{-l'M} \\ &= \sum_{k'=0}^{M-1} \beta_k e^{\left(j\frac{2\pi k'k}{M}\right)} z^{-k'} G^{k'}(z^M) \end{aligned} \tag{3.12}$$

From Eq. (3.13), the FBMCs modulator the poly-phase implementation structure is obtained, as given in Figure 3.6.

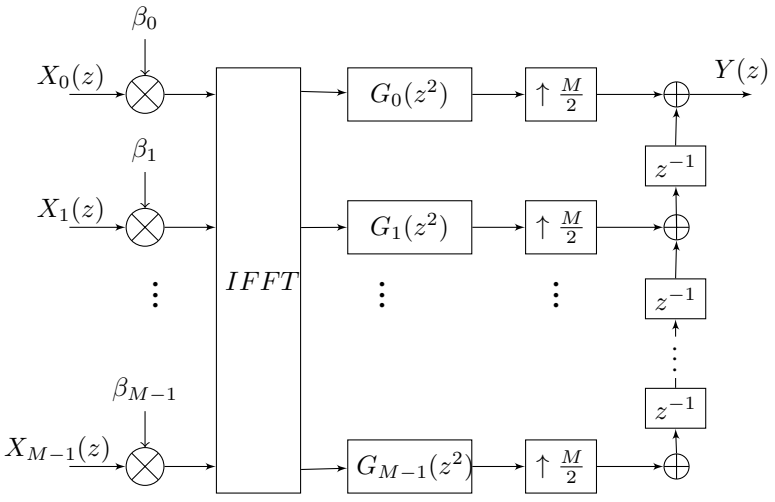

FIGURE 3.6: Efficient synthesis filter bank poly-phase implementation.

3.2.2.2 Analysis filter bank poly-phase structure

The analysis filters are expressed using accurately the similar derivation as the synthesis filters. Therefore,the k^{th} analysis filter poly-phase decomposition can be directly expressed as follows

$$\begin{aligned} F_k[z] &= \sum_{m=0}^{L-1} g(m) e_k[m] z^{-m} \\ &= \sum_{k'=0}^{M-1} \beta_k e^{\left(j\frac{2\pi k' k}{M}\right)} z^{-k'} G^{k'}(z^N) \end{aligned} \tag{3.13}$$

The AFB can be understood to consist of β_k-multipliers, delay chain, IDFT, type-1 poly-phase filters, and down-samplers by $M/2$. Obviously, the down-samplers by $M/2$ are moved trough β_k-multipliers, IDFT, and polyphase filters. The poly-phase implementation structure that is the same with synthesis filter bank is resulted as shown in Figure 3.7. In the reversed order the similar main processing blocks can be done as in the case of synthesis filter bank are done.

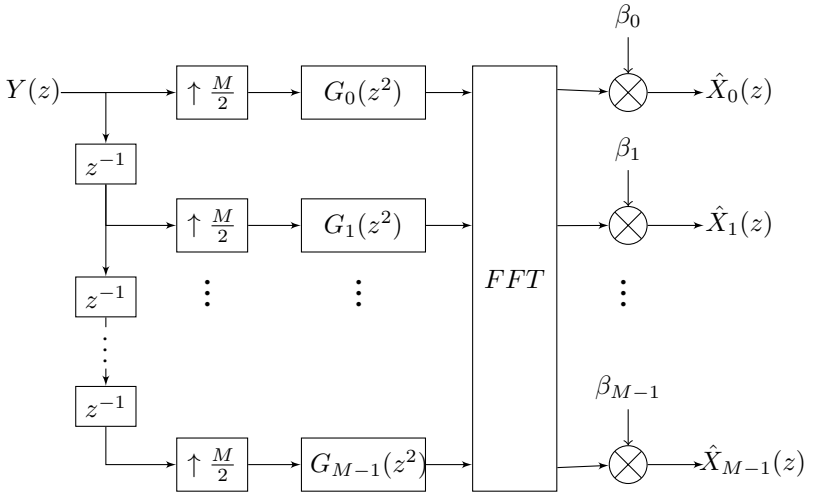

FIGURE 3.7: Efficient of analysis filter bank poly-phase implementation.

3.2.3 Prototype filter

The key element in the complex modulated filter banks is prototype filter because all SFB and AFB are the corresponding low pass prototype filter frequency response frequency shifted versions. Different prototype filters are intended for their matching applications. Some the prototype filters examples are Rectangular

window, the square root raised cosine (RRC) filter, Hermite, PHYDYAS prototype filter and Isotropic orthogonal transform algorithm (IOTA) prototype filter. The different prototype filters impulse response comparison is shown in Fig. 3.9. Obviously, compared to the other filters type, PHYDYAS filter offers the best localization in time and frequency . The RRC filters response continues in time domain and cannot be a good choice for using in FBMC systems. In this sense, the filter bank system quality be contingent mostly on the prototype filter properties. The prototype filters that is more often used in this thesis is PHYDYAS filter. The prototype filter is selected to be a causal and real valued symmetric FIR filter with high frequency selectivity in PHYDYAS project.

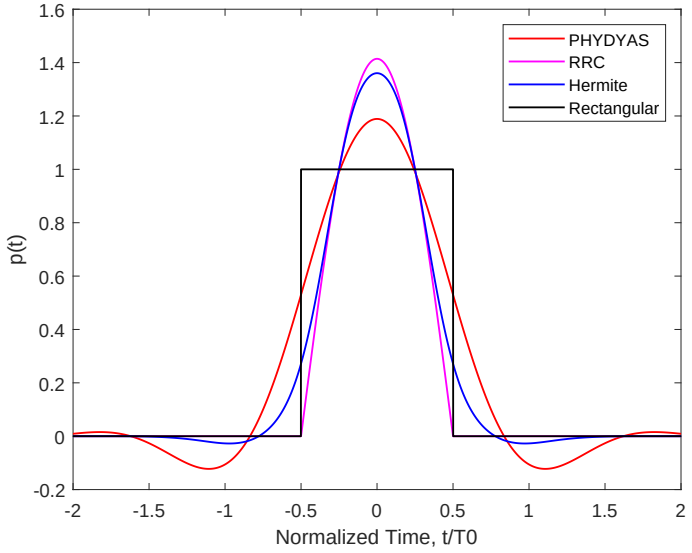

FIGURE 3.8: Impulse response of different prototype filters

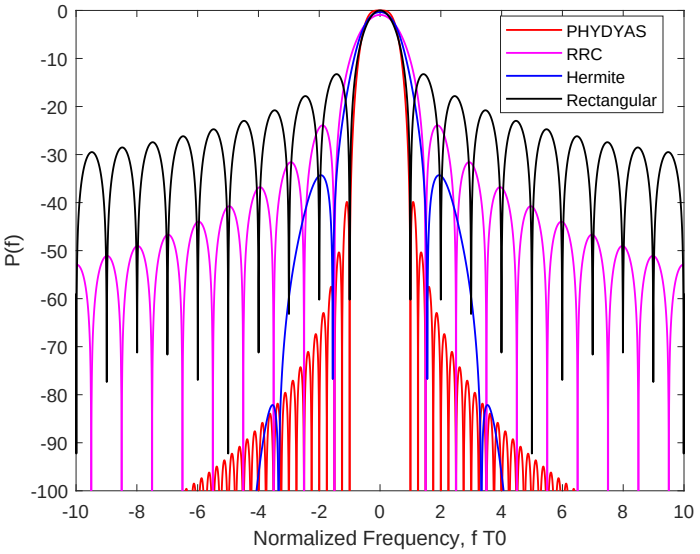

FIGURE 3.9: Frequency response of different prototype filters

3.2.3.1 PHYDYAS filter

PHYDYAS filter is the one intended for dynamic spectrum access and cognitive radio (PHYDYAS) European project in the physical layer [34]. It was introduced by Bellanger in [40]. The project is established on the frequency sampling technique, which provides the benefit of using a closed-form demonstration that comprises only a few adaptable design parameters. This technique idea is first to derive the continuous frequency response $G(f)$ through the interpolation formula of the anticipated frequency response samples G_k, that are consistently move apart at the frequency points $f_k = \frac{k}{OT}$ where T is the symbol period and O is the overlapping factor. That is:

$$G(f) = \sum_k G_k \frac{sin(\pi(OTf - k))}{\pi(OTf - k)} \tag{3.14}$$

Then, the prototype filter continuous impulse response is obtained by taking $G(f)$ the inverse Fourier transform, which resulting in:

$$g(t) = \sum_k G_k e^{j2\pi \frac{kt}{OT}} \tag{3.15}$$

The overlapping factor is selected to be $O = 4$, and the frequency coefficients G_k are selected according to the Nyquist theory and are enhanced to offer the maximum frequency selectivity and reduce the total interference which creates from the filter bank structure for the PHYDYAS prototype filter [41]. Thus, for the PHYDYAS filter, the frequency coefficients G_k selected are shown by [40]:

$$\begin{cases} G_0 = 1,\ G_1 = 0.971960,\ G_2 = \frac{1}{\sqrt{2}},\ G_3 = \sqrt{1 - G_1^2} = 0.235147 \\ G_k = 0,\ for\ k > 3 \\ G_k = G_{-k},\ for\, k < 0\ (To\ obtain\ a\ real - valued\ filter) \end{cases} \tag{3.16}$$

Therefore, the time-continuous impulse response of the PHYDYAS prototype filter is given by:

$$g(t) = 1 + 2\sum_{k=1}^{O-1} G_k \cos\left(2\pi \frac{kt}{OT}\right), for |t| \leq OT. \tag{3.17}$$

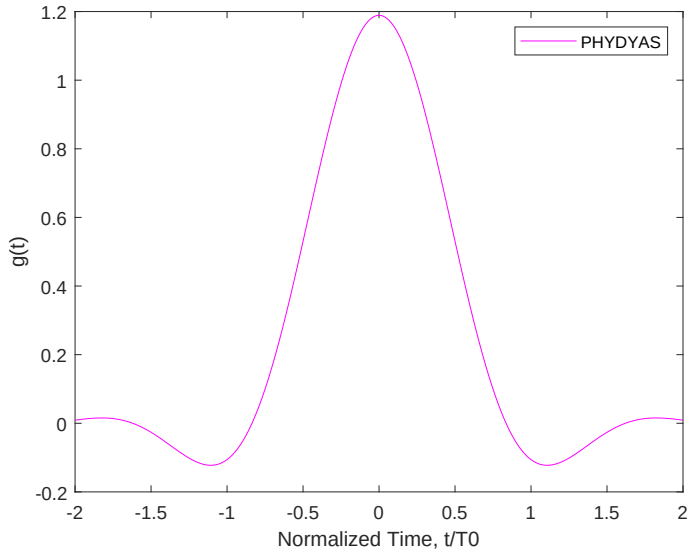

FIGURE 3.10: PHYDYAS prototype filter

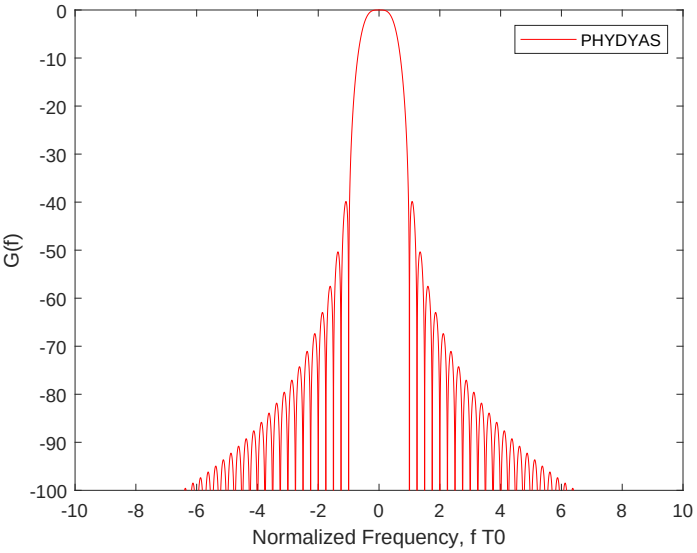

FIGURE 3.11: PHYDYAS prototype filter frequency response.

where $G_k, k \in \{1, 2, ..., O-1\}$, are given in (3.16), for an overlapping factor of O = 4. The discrete-time prototype filter with OM length is gained by sampling $g(t)$, as shown follows:

$$g(m) = g(mT_s) = 1 + 2\sum_{k=1}^{O-1} G_k \cos\left(2\pi \frac{km}{OM}\right), m = 0, 1, ..., OM-1. \quad (3.18)$$

3.2.4 Channel Estimation and Equalization

The effect of wireless channels on the system performance as it is well known it is greatly large. The FBMC/OQAM systems do well if accurate channel information is there. Thus, channel equalization and estimation perform a key role in FBMC/OQAM systems. However, the FBMC/OQAM systems orthogonality condition only holds in the real-number field, which causes the intrinsic imaginary interference to real transmitted symbols at the receiver, which different from OFDM systems. Thus, the conventional channel estimation techniques engaged in OFDM systems cannot be used in OQAM/FBMC systems directly because the intrinsic imaginary interference has to be assumed for the channel estimation patterns in FBMC/OQAM systems.

Presently, the FBMC/OQAM systems channel estimation can be categorized into two categories. These are time-domain channel estimation [[51]- [53]] and channel estimation in frequency-domain [[43]- [50]]. The channel estimation methods in frequency domain are very simple and single-tap equalizers can be engaged for channel equalization in FBMC/OQAM systems similar to OFDM systems. However, in FBMC/OQAM systems, frequency domain channel estimation techniques work well only for the small channel delay spread. The frequency-domain channel estimation methods performances degrade seriously for the relatively large channel delay spread. The time-domain channel estimation techniques are anticipated, that work well even for the large channel delay spread to solve this problem. As for the equalization, inappropriately, for the large channel delay spread, simple single-tap equalizers cannot be engaged for channel equalization. Therefore, in FBMC/OQAM systems, channel estimation and equalization require more surveys.

Chapter 4

Analysis and Implementation of FBMC/OQAM Massive MIMO System with Channel Equalizer

FBMC/OQAM is a multicarrier modulation scheme that precents a specially designed prototype filter which is well localized both in frequency and time domain to an OFDM. It uses offset QAM for modulating each sub-carriers. This prototype filter provides lower spectral leakage and the robustness against multipath channels for FBMC without the use of CP unlike conventional CP based OFDM system [64]. The baseband discrete signal for OFDM can be calculated as [34]

$$s(m) = \frac{1}{\sqrt{M}} \sum_{k=0}^{M-1} \sum_{n=-\infty}^{\infty} s_{k,n} g[m - nM] e^{j\frac{2\pi km}{M}} \tag{4.1}$$

where, k is the sub-carrier index, $s_{k,n}$ is a quadrature modulated symbol which is the data transmitted on the k^{th} sub-carrier of the n^{th} OFDM symbol, M is the total sub-carriers number in a OFDM symbol, the factor $\frac{1}{\sqrt{M}}$ is introduced for power normalization, and g is the rectangular window function which isolates the sub-channels, with its time domain coefficients expressed as

$$g(m) \quad = \begin{cases} \frac{1}{\sqrt{T}}, & if\ |m| \leq \frac{T}{2}, \\ 0, & if\ |m| > \frac{T}{2} \end{cases} \tag{4.2}$$

where $T = \frac{1}{\Delta f} = MT_s$ is the OFDM symbol duration, T_s is the sampling interval and Δf is the subcarrier spacing. A cyclic prefix(CP) with length of L_{cp} is added to the OFDM symbol whose length is equal or greater than the channel delay

spread to eliminate the ISI and ICI. However, the signal to noise ratio (SNR) is reduced by a factor $\alpha = \frac{M}{M+L_{cp}}$ due to this CP. Unlike OFDM, in a FBMC system, each sub-carrier is modulated with a real-valued symbol to fulfill the orthogonality requirement. The FBMC system transmit a real symbol every half symbol duration to maintain the same data rate as OFDM system without CP i.e. $T = 2$, which is gives so called FBMC/OQAM system. This is done at the transmitter side where each complex data symbol $a_{k,n}$, is divided into real/in-phase ($a^I_{k,n}$) and imaginary/quadrature phase ($a^Q_{k,n}$) components. If T is complex OFDM symbol duration without CP, then $\tau_0 = \frac{T}{2}$ is the real FBMC/OQAM symbol duration. However, the FBMC/OQAM sub-carrier spacing υ_0 is equal to OFDM sub-carrier spacing i.e., $\upsilon_0 = \Delta f$. Thus, in the case of the FBMC/OQAM system, $\tau_0\upsilon_0 = \frac{1}{2}$ is considered, which means that the sub-carriers density in time frequency strategy is twice greater in FBMC/OQAM than the conventional OFDM, where $T\Delta f = 1$. The two real-valued symbols are carried in FBMC/OQAM system each with duration $\frac{T}{2}$ instead of symbol signals carried by one complex-valued OFDM symbol with duration T. Hence, the FBMC/OQAM spectral efficiency is similar to that of conventional OFDM without CP.

4.1 FBMC/OQAM modulation

To reduce some shortcoming of CP-OFDM such as the poor spectrum localization, a prototype filter (or finite pulse shape filter) g[m] that is different from the rectangular one with flat edges is used [15]. This gives the filter-bank multicarrier (FBMC) systems and the filtered OFDM [42, 33, 55, 56]. Then again, due to any guard interval used, a spectral efficiency losses with symbol density ($\rho < 1$) is there as in OFDM due to the CP. Hence, to remove this drawback, a multi-carrier systems with symbol density ($\rho = 1$) is presented. However, theoretically, the Balian Low theorem verified that it is impossible to obtain a prototype function being well-localized in time and frequency, and meeting in the time being the orthogonality princinple and a symbol density of ($\rho = 1$) [54]. Therefore, to satisfy these goals, the orthogonality principle must relax and limited it to the real field. Therefore, instead of a QAM, the transmitted data selected from a PAM constellation must be real-valued or purely imaginary in order to demodulate the transmitted data at the receiver side. But, a two real-valued (one complex-valued symbol) symbol density the time-frequency plane per area unit is selected to sustain equal desired data rate [15].

4.1.1 FBMC/OQAM principle

The main concept in the FBMC/OQAM is to transmit real-valued (offset QAM) symbols instead of conventional QAM(complex symbols) ones. Certainly, each complex signal symbol $a_{k,n}, where, k = 0, 1, ..., M-1$ carried at rate F = 1/T by the k^{th} sub-stream, is separated into its in-phase (real part); $a^{I}_{k;n}$ and quadrature (imaginary part) $a^{Q}_{k,n}$ parts at the transmitter side. These possibly will be supposed of as the PAM pair sequences components that are formerly transmitted using a time offset T=2. Through the time and frequency axes, any adjacent PAM symbols pair are transmitted using a $+\pi/2$ phase shift. Where $a_{k,n}$ is the transmitted PAM

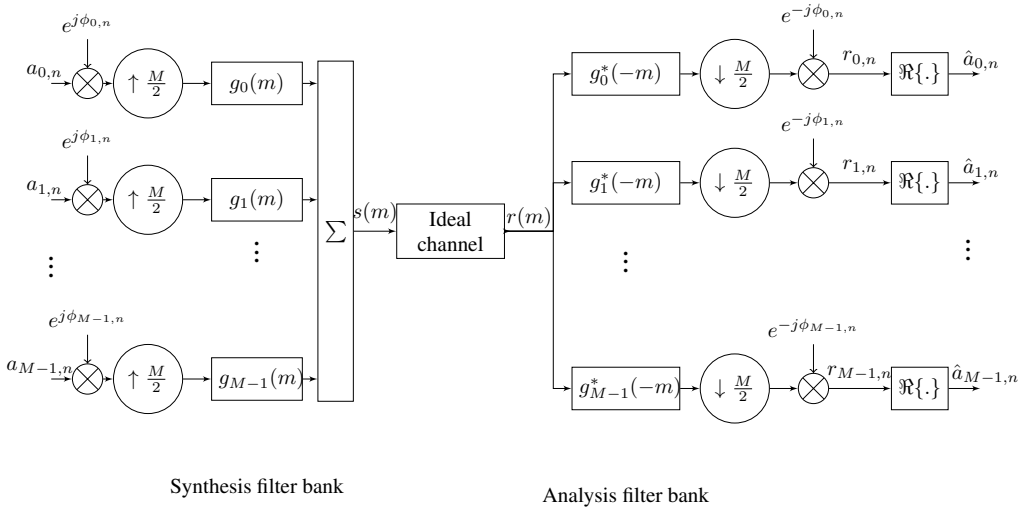

FIGURE 4.1: The transceiver discrete time of the FBMC/OQAM block diagram

symbol, at nT=2 time instant and the k^{th} sub-carrier, which is a QAM (complex) symbol is either the in-phase or the quadrature part. And, assume that g[m] is a causal prototype filter with length $L_g = OM$, where O is the overlapping factor and M is the total number of subcarriers [40]. The FBMC/OQAM baseband transmitted signal in discrete-time can be presented as [28]:

$$s(m) = \sum_{k=0}^{M-1} \sum_{n=-\infty}^{\infty} a_{k,n} g[m - nM/2] e^{j\frac{2\pi k}{M}(m-D/2)} e^{j\phi_{k,n}}, \tag{4.3}$$

where D=2 is a delay term which depends on the prototype filter length L_g and in this case $D = L_g - 1 = OM - 1$. $\phi_{k,n}$ is phase term that cover $\pi/2$ phase shift between neighboring transmitted PAM symbols through the time and frequency axes, and can be specified by [57]:

$$\phi_{k,n} = \frac{\pi}{2}(n+k) \tag{4.4}$$

The equation in(4.3) can be written in a simpler manner as:

$$s(m) = \sum_{k=0}^{M-1} \sum_{n} a_{k,n} g_{k,n}[m] \tag{4.5}$$

where g[m] is defined by

$$g_{k,n}[m] = g[m - nM/2] e^{j\frac{2\pi k}{M}(m-D/2)} e^{j\phi_{k,n}} \tag{4.6}$$

The demodulated symbol over the k^{th} sub-carrier and the n^{th} instant can be determined using the inner product of s[m] and $g_{k,n}[m]$, assuming a free of noise and distortion less channel:

$$\begin{aligned} r_{k,n} &= \langle s(m), g_{k,n} \rangle = \sum_{m=-\infty}^{+\infty} s(m) g^*_{k,n}[m] \\ &= \sum_{k'=0}^{M-1} \sum_{n'=-\infty}^{+\infty} a_{k',n'} \sum_{m=-\infty}^{+\infty} g_{k',n'}[m] g^*_{k,n}[m] \end{aligned} \tag{4.7}$$

Then, the trans-multiplexer impulse response from the equation (4.7)is expressed by assuming that only a unit impulse is transmitted in a frequency-time position (k_0, n_0), as follows:

$$\begin{aligned} r_{k,n} &= \sum_{m=-\infty}^{+\infty} g_{k_0,n_0}[m] g^*_{k,n}[m] \\ &= \sum_{m=-\infty}^{+\infty} g[m] g[m - \Delta n M/2] e^{j\frac{2\pi}{M}\Delta k(D/2-m)} e^{j\pi(\Delta k + k_0)\Delta n} e^{j\pi(\Delta k + \Delta n)}, \end{aligned} \tag{4.8}$$

where $\Delta k = k - k_0$ and $\Delta n = n - n_0$. so, the trans-multiplexer impulse response be contingent strongly on the prototype filter g[m]. The prototype filter must be intended such that it fulfills the orthogonality principles limited to the real field

$$\Re\left\{\sum_{m=-\infty}^{+\infty} g_{k',n'}[m]g_{k,n}^{*}[m]\right\} = \delta_{k,k'}\delta_{n,n'} \tag{4.9}$$

Therefore, equation (4.7) can be rewritten as

$$r_{k,n} = a_{k,n} + \underbrace{\sum_{(k',n')\neq(k,n)} a_{k',n'} \sum_{m=-\infty}^{+\infty} g_{k',n'}[m]g_{k,n}^{*}[m]}_{I_{k,n}} \tag{4.10}$$

where $I_{k,n}$ is the FBMC/OQAM system inherent inter-symbol interference. Then all the transmitted symbols $a_{k',n'}$ are real-valued symbols and due the real orthogonality principle (4.9), and $I_{k,n}$ is ISI term and purely imaginary i.e. $I_{k,n} = ju_{k,n}$ with $u_{k,n}$ is real-valued. Consequently, equation(4.10) can be rewritten as:

$$r_{k,n} = a_{k,n} + ju_{k,n}, \tag{4.11}$$

and the transmitted real-valued symbols $a_{k,n}$ is recuperated fairly by retrieving the received demodulated signal $r_{k,n}$ real part.

$$\hat{a}_{k,n} = \Re\{r_{k,n}\} = a_{k,n}. \tag{4.12}$$

4.1.2 FBMC/OQAM in multipath channel

However, if a realistic channel for transmission is considered , the real orthogonality condition in (4.9) will be lost. The consecutive transmitted symbols will overlay as result of the multi-path channel effect because FBMC/OQAM does not use any guard interval. The time-invariant channel is assumed for derivation simplicity. It is also assume that the number of sub-carriers M is sufficiently large,as in the case of CP-OFDM, i.e. $L_h << M$ where L_h is the length of the discrete channel response so that the channel is seen as a flat fading at each sub-channel. The discrete time baseband version of the received signal,after passing through the

multipath channel and noise taken apart can be written as follows:

$$\begin{aligned} r[m] &= (h * s)[m] \\ &= \sum_{l=0}^{L_h-1} h[l]s[m-l] \\ &= \sum_{n=-\infty}^{+\infty} \sum_{k=0}^{M-1} a_{k,n} \sum_{l=0}^{L_h-1} h[l]g_{k,n}[m-l] \\ &= \sum_{n=-\infty}^{+\infty} \sum_{k=0}^{M-1} a_{k,n} e^{j\frac{2\pi k}{M}(m-D/2)} e^{j\phi_{k,n}} \underbrace{\sum_{l=0}^{L_h-1} h[l]g[m-l-nM/2]e^{-j2\pi\frac{kl}{M}}}_{\Theta} \end{aligned} \tag{4.13}$$

In the last term Θ, the exponential term $e^{-j2\pi\frac{kl}{M}}$ has fast variations for $l \in \{0, ..., L_h - 1\}$ and cannot be constant over this set (or interval $[0, L_h]$). However, $g[m-l-nM/2]$ may have only relatively slow variations when $l \in \{0, ..., L_h - 1\}$. Actually, compared to the filter bandwidth, the coherence bandwidth is large ($L_h << L_g = OM$), which also means that time variations of g are necessarily very limited [57]. Therefore, we can assume that $g[m-l-nM/2] \approx g[m-nM/2]$ for $l \in \{0, ..., L_h - 1\}$.
Then, Θ can be approximated by:

$$\Theta \approx g[m - nM/2] \sum_{l=0}^{L_h-1} h[l]e^{-j2\pi\frac{kl}{M}} \tag{4.14}$$

Setting

$$h_{k,n} = \sum_{l=0}^{L_h-1} h[l]e^{-j2\pi\frac{kl}{M}} \tag{4.15}$$

where $h_{k,n}$ is the channel frequency response at subcarrier k and at time index n, and taking into account the presence of an AWGN term, we can simplify (4.13) as:

$$\begin{aligned} r[m] &= \sum_{n=-\infty}^{+\infty} \sum_{k=0}^{M-1} h_{k,n}a_{k,n}g[m - nM/2]e^{j\frac{2\pi k}{M}(m-D/2)}e^{j\phi_{k,n}} + \gamma[m] \\ &\approx \sum_{n=-\infty}^{+\infty} \sum_{k=0}^{M-1} h_{k,n}a_{k,n}g_{k,n}[m] + \gamma[m] \end{aligned} \tag{4.16}$$

where$\gamma[m]$ is the AWGN term with variance σ^2. The demodulation of the received signal at time-frequency position (k, n) provides a complex symbol denoted by $r_{k,n}$ at the receiver side(see 4.1). The demodulated signal after matched filtering and phase compensation, and before taking the real part can be expressed as :

$$\begin{aligned} r_{k,n} &= \sum_{m=-\infty}^{+\infty} r[m]g_{k,n}^*[m] \\ &= \sum_{n'=-\infty}^{+\infty}\sum_{k'=0}^{M-1} h_{k',n'}a_{k',n'} \underbrace{\sum_{m=-\infty}^{+\infty} g_{k',n'}[m]g_{k,n}^*[m]}_{\langle g_{k',n'},g_{k,n}\rangle} + \underbrace{\sum_{m=-\infty}^{+\infty}\gamma[m]g_{k,n}^*[m]}_{\gamma_{k,n}} \\ &= \sum_{n'=-\infty}^{+\infty}\sum_{k'=0}^{M-1} H_{kk',nn'}a_{k',n'} + \gamma_{k,n} \end{aligned} \tag{4.17}$$

where $\gamma_{k,n}$ is a noise term at the demodulator output and the interference coefficient $H_{kk',nn'}$ can be calculated according to.

$$H_{kk',nn'} = h_{kk'}(n - n^{'})e^{j(\phi_{k',n'}-\phi_{k,n})} \tag{4.18}$$

$$h_{kk'}(n) = (g_{k'}(m) * h(m) * g_k^*(-m))_{\downarrow\frac{M}{2}} \tag{4.19}$$

Where, $h_{kk'}(n)$ is the equivalent channel impulse response between the transmitted symbols at sub-carrier $k^{'}$ and the received symbols at sub-carrier k. It includes the effects of the transmitter and the receiver pulse-shaping,and the multi-path channel. $\frac{M}{2}$ denotes decimation with the rate of M/2. The demodulated symbol $r_{m,n}$ undertakes interference coming from other time-frequency symbols according to (4.17). The prototype filter $g(m)$ is designed to be well localized in time and frequency practically. As a result, the interference is reduced to a small number of neighboring symbols around the desired time-frequency point (k, n). It is usually assumed that the channel length, L_h is relatively small compared to the symbol period, M/2, in order to develop a simple equalizer to combat the frequency-selective channel effect. Affording to the real orthogonality condition (4.9), then it can be written as:

$$r_{k,n} = h_{k,n}a_{k,n} + \underbrace{\sum_{(k',n')\neq(k,n)} h_{k',n'}a_{k',n'}\langle g_{k',n'}, g_{k,n}\rangle}_{\bar{I}_{k,n}} + \gamma_{k,n}, \tag{4.20}$$

where $\bar{I}_{k,n}$ is a complex interference term as $h_{k',n'}$ are complex coefficients. The prototype filter g[m] is supposed to be well-localized in time-frequency domain, which

means that it exists a finite set $\Omega_{k,n}$ of neighboring positions around the considered one which can be defined as $\Omega_{k,n} = \{(k^{'}, n^{'})/(k^{'}, n^{'}) \notin \Omega_{k,n} \Longrightarrow \langle g_{k^{'},n^{'}}, g_{k,n} \rangle = 0\}$. Then, the size of $\Omega_{k,n}$ depends only on how the prototype filter g[m] is designed. Setting $\Omega^{*}_{k,n} = \Omega_{k,n} - (k, n)$, the complex interference term $\bar{I}_{k,n}$ can be rewrite as:

$$\bar{I}_{k,n} = \sum_{(k^{'},n^{'}) \in \Omega^{*}_{k,n}} h_{k^{'},n^{'}} a_{k^{'},n^{'}} \langle g_{k^{'},n^{'}}, g_{k,n} \rangle \tag{4.21}$$

Then, the objective is to design a filter so conveniently well-localized that we can consider the channel coefficients $h_{k,n}$ as constant within $\Omega_{k,n}$. That is, $(k^{'}, n^{'}) \notin \Omega_{k,n} \Longrightarrow h_{k^{'},n^{'}} \approx h_{k,n}$. In this case, we can write

$$\begin{aligned} \bar{I}_{k,n} &\approx h_{k,n} \sum_{(k^{'},n^{'}) \in \Omega^{*}_{k,n}} a_{k^{'},n^{'}} \langle g_{k^{'},n^{'}}, g_{k,n} \rangle \\ &\approx j h_{k,n} u_{k,n}, \end{aligned}$$

where the last equality is obtained according to (4.9), and $u_{k,n}$ is a real-valued interference term. Finally, substituting this last expression into (4.18), we obtain the demodulated signal expressed as:

$$r_{k,n} \approx h_{k,n}(a_{k,n} + j u_{k,n}) + \gamma_{k,n}, \tag{4.22}$$

Where, $h_{k,n} = \sum_{l=0}^{L_h - 1} h[l] e^{-j2\pi \frac{kl}{M}}$ is the channel frequency response at the center of the k^{th} sub-carrier. The term $u_{k,n}$ is the intrinsic interference and it is purely imaginary. And, it represents the role of the inter-symbol interference (ISI) and inter-carrier interference (ICI) from the adjacent time-frequency symbols around the desired point (k, n). The effect of channel distortions can be compensated using a single-tap equalizer per sub-carrier based on (4.22). After taking equalization, what remains is the real-valued data symbol $a_{k,n}$, the imaginary term $u_{k,n}$, and the noise impact. Generally, an estimated of $a_{k,n}$ can obtain and the intrinsic interference can remove by taking the real part from the equalized symbol. The performance of the above single-tap equalization primarily depends on the validity of the assumption that the channel length is much smaller than the symbol duration, but the assumptionis not accurate in highly frequency-selective channels. More advanced equalization methods are deployed to counteract the channel distortions in highly frequency-selective channels [28].

4.2 Massive MIMO Systems

The 5G communication system is a system that expected to enhances high capacity, high data rate, low complexity and ultra reliable low latency [59]. A new technology including massive MIMO, non-orthogonal multiple access (NOMA), visible light communication, millimeter wave communication will be introduced to achieve these expectation.

when consumption of total transmitted power is remain stable, massive MIMO gives improved communication capacity significantly. As a result, spectral efficiency are enhanced significantly in massive MIMO systems, which can be derived from the system achievable capacity improvement, compared to traditional point-to-point (P2P) system [61]. Moreover, in spatial domain, massive amount of freedom degrees will facilitate allocation of power, contributing to energy efficiency. Hence, it is a core of 5G technology in the future.

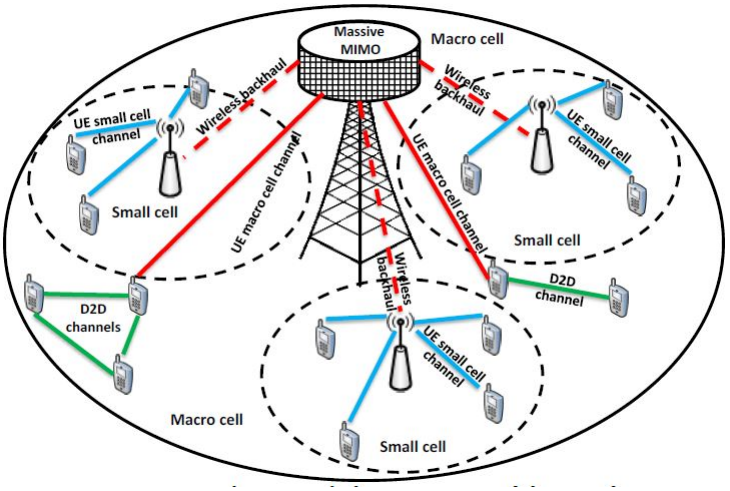

FIGURE 4.2: Architecture of a heterogeneous mobile network [65]

4.2.1 Linear detector Schemes

In massive MIMO systems, to eliminate inter-user interference and to maximize SNR, linear detectors are used at the receiver side. Therefore, the system can be simplified as a Single-input-to-Single-output (SISO) systems when the amount of transmitted antennas approaches to infinity. Moreover, in massive MIMO systems, to optimize spectral resources, Linear detectors are used in order to reduce the system complexity, diminish noise effect and optimize stream data transmission based on channel state information (CSI) at the receiver side. There are three

common linear combiners schemes, including MRC, ZF and MMSE.

1) Maximum combining-ratio (MRC)

This detector is detector that maximize SNR by Looking for at the receiver combiner to maximize the power. For massive MIMO systems, MRC is considered as a possible linear reception scheme since it can be applied in a distributed manner.Its mathematical is given by

$$W_k = H_k D_k^{-1}$$

Moreover, it has a good performance in the low SNR regime, even upcoming to optimal performance as a number of antennas increases infinitely. However, as the SNR increase, massive MIMO systems based on this detector undergo serious inter-user interference [58].

2) Zero-forcing(ZF)

ZF is linear detector that eliminate inter-user interference by projecting the received signals into the orthogonal elements. It does not take noise into consideration. The system that depend on ZF detector scheme has a poor performance in low SNR regime and the performance in high-SNR regime approaches to optimal [58]. It can be written as

$$W_k = H_k (H_k^H H_k)^{-1}$$

3) Minimum Mean-Square Error (MMSE)

It is used to eliminate noise and inter-user interference and relatively it has higher system complexity compared to MRC and ZF.

$$W_k = H_k (H_k^H H_k + \sigma_\gamma^2 I_K)^{-1}$$

MRC has lowest complexity among three of these linear detectors schemes when see from mathematical perspective. It needs perfect channel state information [58]. From figure 4.3, it is clearly that MMSE system has the good performance through the whole power SNR in terms of capacity among three of them. The achievable data rate is 19 bits/s/Hz at SNR is equal to 0dB and it increases as the transmitted power increases, correspondingly. ZF has a similar performance with MMSE, but, it has a poor performance in low SNR regime because it does not take noise into account. The achievable data rate of ZF increases when SNR is larger than 10dB, significantly and even it approaches to that of MMSE in high SNR regime.

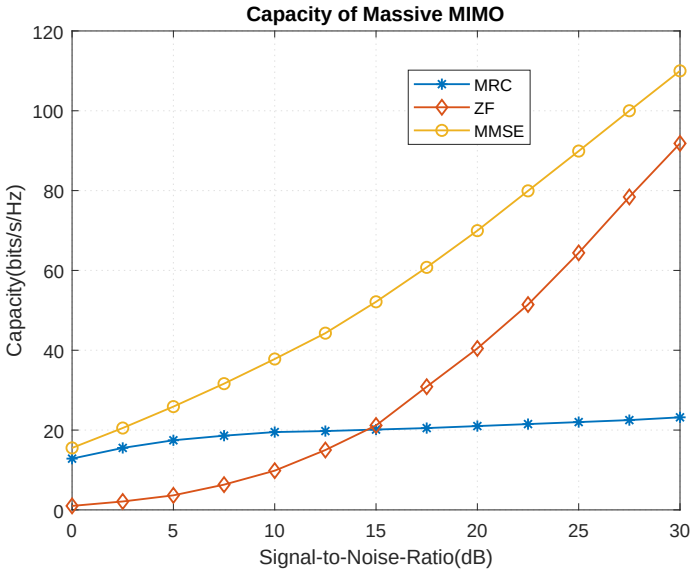

FIGURE 4.3: Linear detectors comparison

Due to less inter-users interference, MRC has a relatively good achievable data rate, which is approaching to MMSE in low SNR regime. However, due to high interference from individuals users, the capacity almost saturate when SNR is larger than 10 dB.

From figure 4.3, therefore, MMSE has the best performance of a system in terms of achievable data rate with known perfect channel state information. From the remaining two detectors schemes, ZF has a best performance in high SNR regime, and MRC has a best performance in low SNR regime. And, ZF do not requires perfect CSI and MRC has the lowest complexity.

4.3 FBMC/OQAM Massive MIMO systems

In this section, Massive MIMO systems are applied to FBMC/OQAM and for signals detection, the three linear combiners, namely, maximum-ratio combining (MRC), zero-forcing (ZF), and minimum mean-square error (MMSE) are considered. As it has shown in section 4.1.2, in the case of a SISO transmission between an antenna j and a received antenna i for FBMC/OQAM systems, if $a_{k,n}^{(j)}$ is the transmitted real data at time n and at frequency k then the demodulated signal $r_{k,n}^{(i)}$ is given by:

$$r_{k,n}^{(i)} \approx h_{k,n}^{(ij)}(a_{k,n}^{(j)} + ju_{k,n}^{(j)}) + \gamma_{k,n}^{(i)}, \tag{4.23}$$

where $h_{k,n}^{(ij)}$ is the channel coefficient from the transmit antenna j to the receive antenna i at frequency k and time instant n. $\gamma_{k,n}^{(i)}$ is the noise component at antenna i and at time-frequency (n,k). $u_{k,n}^{(j)}$ is the interference term as given in (4.10). In the case of Mssive MIMO transmission, the signals received with each antennas at the BS antennas are linear combined using the channel frequency coefficients. However, even with number of an infinite BS antennas, it leads to a residual interference. As a result, the SINR is limited to a certain deterministic value, and SINR values cannot be increased as the number of BS antennas increases. Due to upper bounded of the SINR by a certain deterministic value as the number of BS antennas increases large, channel capacity performances cannot increase effectively with the number of BS antennas. Through a simple channel equalizer, this problem can be resolved.

To solve this problem, a single-cell massive MIMO system that has a BS equipped with N number of antenna elements and K single-antenna mobile terminals (MTs) which are simultaneously communicating in the case of the uplink transmission are considered [7]. Also, the results and proposed technique are inconsequentially applicable to the down-link transmission.
Let $s_i(l)$ represent the terminal i the transmit signal. At the j^{th} BS antenna, the received signal can be obtained as

$$r_j(l) = \sum_{i=0}^{K-1} s_i(l) * h_{j,i}(l) + \gamma_i(l), \tag{4.24}$$

where $h_{j,i}(l)$ is the channel impulse response between the i^{th} terminal and the j^{th} BS antenna, and $\gamma_i(l)$ is the additive noise at the input of the j^{th} BS antenna. This additive noise signal samples $\gamma_i(l)$ are independent and identically distributed (i.i.d.) random variables with $CN(0, \sigma_\gamma^2)$. A channel power delay profile (PDP)is used to model the corresponding channel responses $\rho(l), l = 0, ..., L-1$. The channel tap $h_{j,i}(l)$, $l \in 0, ..., L-1$, follows a $CN(0, \rho(l))$ is assumed and these taps are assumed to be independent. The channel PDP is normalized such that $\sum_{i=0}^{L-1} \rho(l) = 1$. Moreover, let consider that the average transmitted power is equal to one, i.e.,$E\{|s_i(l)|^2\} = 1$ for each terminal is considered. As a result, using above channel model, at the input of the BS antennas, the signal-to-noise ratio (SNR) can be calculated as $SNR = 1/\sigma_\gamma^2$. To simplify the analysis , the BS has a perfect channel state information(CSI) knowledge is considered .

Therefore, in the MIMO context, when K users are used to transmit K numbers of real data symbols and N antennas are used to collect the transmitted signals,

the FBMC received signal at the j^{th} receive antenna and at a given time-frequency position (k, n) is expressed by:

$$r_{k,n}^{(j)} \approx \sum_{i=0}^{K-1} h_{k,n}^{(ji)}(a_{k,n}^{(i)} + ju_{k,n}^{(i)}) + \gamma_{k,n}^{(j)}, \tag{4.25}$$

Finally, the system matrix formulation can be expressed as:

$$\underbrace{\begin{bmatrix} r_{k,n}^{(1)} \\ \vdots \\ r_{k,n}^{(N)} \end{bmatrix}}_{r_{k,n}} = \underbrace{\begin{bmatrix} h_{k,n}^{(11)} & \cdots & h_{k,n}^{(1K)} \\ \vdots & \ddots & \vdots \\ h_{k,n}^{(N1)} & \cdots & h_{k,n}^{(NK)} \end{bmatrix}}_{H_{k,n}} \underbrace{\begin{bmatrix} a_{k,n}^{(1)} + ju_{k,n}^{(1)} \\ \vdots \\ a_{k,n}^{(K)} + ju_{k,n}^{(K)} \end{bmatrix}}_{a_{k,n}+ju_{k,n}} + \underbrace{\begin{bmatrix} \gamma_{k,n}^{(1)} \\ \vdots \\ \gamma_{k,n}^{(N)} \end{bmatrix}}_{\gamma_{k,n}} \tag{4.26}$$

which yields:

$$r_{k,n} = H_{k,n}(a_{k,n} + ju_{k,n}) + \gamma_{k,n} \tag{4.27}$$

where $H_{k,n}$ is an $(N \times K)$ channel matrix. Using (4.24, 4.25, 4.26, 4.27) and extending (4.17) to the MIMO case, we have

$$r_{k,n} = \sum_{n'=-\infty}^{+\infty} \sum_{k'=0}^{M-1} H_{kk',nn'} a_{k',n'} + \gamma_{k,n} \tag{4.28}$$

where $r_{k,n}$ is an $N \times 1$ vector containing the received symbols corresponding to different BS antennas and time-frequency (k, n) point. $\gamma_{k,n}$ is vector contains the noise contributions through different BS antennas. $a_{k,n}$ is $Kx1$ vector containing all the MTs the data symbols transmitted at the point (k, n). $H_{kk',nn'}$ is an $N \times K$ matrix with its element ji, denoted by $H_{kk',nn'}^{j,i}$, representing the interference coefficient corresponding to the channel $h_{j,i}(l)$. These interference coefficient can be intended similar to(4.18) as

$$H_{kk',nn'}^{j,i} = h_{kk'}^{j,i}(n - n^{'})e^{j(\phi_{k',n'} - \phi_{k,n})} \tag{4.29}$$

$$h_{kk'}^{j,i}(n) = (g_{k'}(m) * h_{j,i}(m) * g_k^*(-m))_{\downarrow \frac{M}{2}} \tag{4.30}$$

A single-tap equalizer per sub-carrier is assumed at the BS. Through an $N \times K$ combining matrix W_k, the elements of $r_{k,n}$ combined and after taking the real part of these combined signal, the transmitted data symbols estimate at BS for all the

MTs can be got as

$$\begin{aligned}\hat{a}_{k,n} &= \Re\left\{W_k^H r_{k,n}\right\} \\ &= \Re\left\{\sum_{n'=-\infty}^{+\infty}\sum_{k'=0}^{M-1} W_k^H H_{kk',nn'} a_{k',n'} + W_k^H \gamma_{k,n}\right\} \\ &= \Re\left\{\sum_{n'=-\infty}^{+\infty}\sum_{k'=0}^{M-1} G_{kk',nn'} a_{k',n'} + \gamma_{k,n}^{'}\right\} \end{aligned} \tag{4.31}$$

where $G_{kk',nn'} = W_k^H H_{kk',nn'}$, and $\gamma_{k,n}^{'} = W_k^H \gamma_{k,n}$. The three linear combiners, namely, maximum-ratio combining (MRC), zero-forcing (ZF), and minimum mean-square error (MMSE) considered can be got as,

$$W_k = \begin{cases} H_k D_k^{-1}, & for\ MRC, \\ H_k (H_k^H H_k)^{-1}, & for\ ZF, \\ H_k (H_k^H H_k + \sigma_\gamma^2 I_K)^{-1}, & for\ MMSE, \end{cases} \tag{4.32}$$

where H_k is the channel coefficients matrix at the center of k^{th} sub-carrier, i.e $H_k^{j,i} =^{\Delta} \sum_{l=0}^{L_h-1} h_{j,i}[l] e^{-j2\pi\frac{kl}{M}}$. In MRC, the matrix D_k is a $K \times K$ diagonal normalized matrix that contains the i^{th} squared norm H_k column on its i^{th} diagonal element, and can be calculated as $[D_k]_{ii} = \sum_{j=0}^{N-1} |H_k^{j,i}|^2$. D_k normalize the MRC output amplitude that grows linearly without a bound as the number of BS antennas N increases. According to the large numbers law, D_k and $H_k^H H_k$ tend to NI_K as the number of BS antennas increases. Then, the above all combiners tend to $\frac{1}{N} H_k$ as the number of BS antennas increases [62]. Therefore, to find the various interference terms as the number of BS antennas N goes to infinity, $W_k = \frac{1}{N} H_k$ is considered. Before continue, let recall some results from probability theory. Let $a = [a_1, ..., a_n]^T$ and $b = [b_1, ..., b_n]^T$ be two random vectors each containing i.i.d. elements. Moreover, assume that q^{th} elements of a and b are correlated according to $E\{a_q^* b_q\} = C_{ab}, q = 1, ..., n$. Consequently, according to the large numbers law, the sample mean of random variable $\frac{1}{n} a^H b = \frac{1}{n} \sum_{q=0}^{n} a_q^* b_q$ converges almost surely to C_{ab} as n tends to infinity.

$G_{kk',nn'}^{ii'}$ is the element ii' of $G_{kk',nn'}$. The elements of $G_{kk',nn'} = W_k^H H_{kk',nn'}$ as the number of BS antennas N goes to infinity, can be obtained using the large numbers law, $G_{kk',nn'}^{ii'}$ congregates almost surely to [22, 23]

$$G_{kk',nn'}^{ii'} \rightarrow E\left\{(H_k^{j,i})^* H_{kk',nn'}^{j,i'}\right\} \tag{4.33}$$

The equation(4.29) is used to compute (4.33) and to determine the correspondent channel impulse response between the conveyed data symbols from transmitter and the demodulated ones at receiver after combining the signals through various BS antennas. This equivalent channel impulse response between the transmitted data symbols of MT $i^{'}$ at sub-carrier $k^{'}$ and the received ones at MT i at sub-carrier k as N increases large, approaches to

$$\begin{aligned} g_{kk'}^{ii'}(n) \rightarrow E\left\{(H_k^{j,i})^* \left(g_{k'}(m) * h_{j,i'}(m) * g_k^*(-m)\right)_{\downarrow \frac{M}{2}}\right\} \\ = \left(g_{k'}(m) * E\left\{(H_k^{j,i})^* h_{j,i'}(m)\right\} * g_k^*(-m)\right)_{\downarrow \frac{M}{2}} \end{aligned} \tag{4.34}$$

What we understood above expression (4.34) is that there is a correlation between the channel frequency coefficient $H_k^{j,i}$ and the channel impulse response $h_{j,i'}(m)$. And, it can be determined as

$$\begin{aligned} E\left\{(H_k^{j,i})^* h_{j,i'}(m)\right\} &= \sum_{l=0}^{L_h-1} E\left\{h_{j,i}^*[l] h_{j,i'}(m)\right\} e^{j2\pi \frac{kl}{M}} \\ &= \rho(l) e^{j2\pi \frac{kl}{M}} \delta_{ii'} = \rho_k(l)\delta_{ii'} \end{aligned} \tag{4.35}$$

Where $\rho_k(l) = \rho(l)e^{j2\pi \frac{kl}{M}}$. Although the multi-user interference and noise effects vanish as the number of BS antennas goes to infinity in the massive MIMO systems in the context of FBMC/OQAM, some residual inter-symbols interference and inter-carriers interference from the same user is not removed. In specific, the equivalent channel impulse response between the transmitted data symbols at sub-carrier $k^{'}$ and the received ones at sub-carrier k for a given user i, approaches to

$$g_{kk'}^{ii'}(n) \rightarrow \left(g_{k'}(m) * \rho_k(l) * g_k^*(-m)\right)_{\downarrow \frac{M}{2}} \tag{4.36}$$

As a result, the SINR converges to(see [23])

$$SINR_{k,n}^i \rightarrow \frac{\Re^2\left\{G_{kk,nn}^{ii}\right\}}{\Re^2\left\{\sum_{n'=-\infty}^{+\infty} \sum_{k'=0}^{M-1} {}_{(k',n')\neq(k,n)} G_{kk',nn'}^{ii'}\right\}} \tag{4.37}$$

Where,$G_{kk',nn'}^{ii} = g_{kk'}^{ii'}(n-n')e^{j(\phi_{k',n'}-\phi_{k,n})}$.

From (4.35), the channel impulse response approaches to zero when $i^{'} \neq i$. Hence, multi-user interference and the noise contribution fades away. However, the channel response approaches to (4.36), when $i^{'} = i$, i.e, the interference from the same

user on itself. Due to the presence of correlation $\rho_k(l)$, even with an infinite BS antennas number, the orthogonality condition in the real domain of (4.9) does not hold anymore. Hence, some residual inter-symbol interference(ISI) and inter-carrier interference (ICI) will there and will make the SINR to converges at the level in (4.37) and the channel capacity cannot increase effectively.

The above discussions and analysis that was made for MRC is also valid for the ZF and MMSE combiners. In specific, using the large numbers law, for the ZF and MMSE combiners, when N increases large,$\frac{1}{N}H_k^H H_k$ goes to I_K, and hence the ZF and MMSE matrices in (4.32) converge to that of the MRC [62]. Therefore, for the ZF and MMSE linear combiners, the same asymptotic SINR value, channel capacity and channel response as for the MRC can be got.

4.3.1 Equalization

As prsented in the previous section, some residual ICI and ISI is there due to the correlation between the combiner taps and the channel impulse responses between the MTs and the BS antennas, even with an infinite number of BS antennas. To resolve this problem, a channel equalizer is designed in order to remove this correlation [23]. The equation (4.36)is the modulated channel PDP, $\rho_k(l)$ which results in the saturation issue. If this problematic term is not exist, the channel response $g_{kk'}^{ii'}(n) = (g_{k'}(m) * g_k^*(-m))_{\downarrow\frac{M}{2}}$ produces the result without any interference which shows $q(m) = g(m) * g^*(m)$ is a Nyquist pulse. The effect of this correlation $\rho_k(l)$ can removed by equalizing the channel and the saturation issue can resolved . Let assume $\rho(\omega)$ is the discrete time Fourier transform (DTFT) of $\rho(l)$. Also, we can define $\rho_k(\omega) = \rho(\omega - 2\pi k/M)$ as the DTFT of $\rho_k(l)$. This implies that one can equalize the effect of $\rho_k(l)$ by presenting a filter $\phi_k(l)$ with transfer function

$$\Phi_k(\omega) = \frac{1}{\rho_k(\omega)} \tag{4.38}$$

in combine with $g_k^*(l)$ to fulfill the anticipated equivalent channel response $g_{kk'}^{ii'}(n) \rightarrow (g_{k'}(m) * g_k^*(-m))_{\downarrow\frac{M}{2}}$ in the asymptotic regime. This combinations modifies the structure of receiver as shown in 4.4.

Using the channel equalizer, as the number of BS antennas goes to infinity, the channel distortions, MUI and noise effects will Vanish, and arbitrarily large SINR values can be accomplished and channel capacity can be effectively increased in the FBMC massive MIMO systems. That means, with the equalizer in (4.38), the distortion due to the channel PDP $\rho_k(l)$ in the equivalent channel impulse

response in (4.36) is avoided. Then, the equivalent channel response goes to an ideal channel. As a result, the ICI and ISI effects will disappear, and the multiuser and the noise effect interference will also goes to zero because the different users channels are independent (4.33). Thus, the result found above analysis is usable for any frequency-selective channel and for the flat channel over the bandwidth of each sub-carrier the equalizer in (4.38) becomes unity.

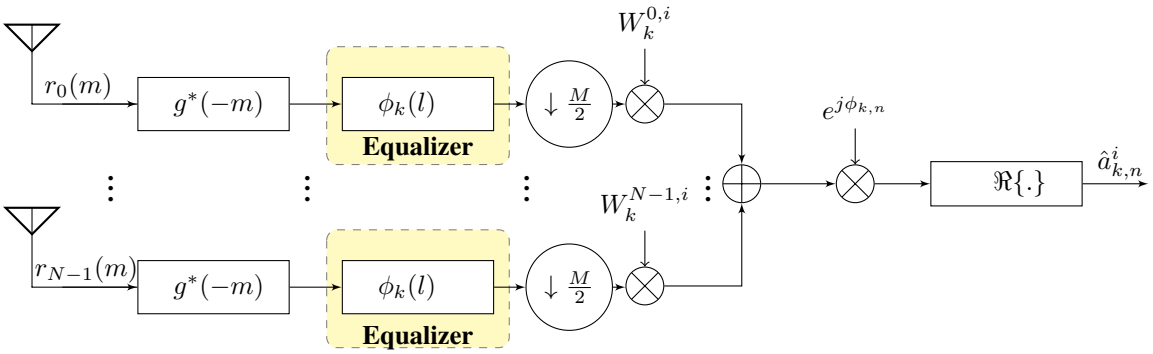

FIGURE 4.4: Block diagram of the simplified receiver with channel equalization.

Hence, for frequency-selective channel, the BS requires to estimate the channel PDP for each terminal to be able to remove the upper bounded limited of SINR. Opportunely, the channel PDP can be approximated in a comparatively simple and feasible manner in massive MIMO systems. In specific, for each terminal, the channel PDP can be obtained by finding the each tap mean power of the respective channel impulse responses through various BS antennas. According to the law of large numbers, as the number of BS antennas grows, this approximatation becomes nearer to the accurate channel PDP. Although the above method resolves the upper bounded problem, the requirement of a isolate filter $\phi_k[l]$ per user per antenna may make this system a very complex receiver and it may not be of practical interest. The multi-rate signal processing techniques is proposed to resolve this complexity issues [23].

4.3.2 Frequency Domain Perspective

The SINR saturation problem of FBMC in massive MIMO was discussed from the time-domain viewpoint in the previous sections. The equivalent channel impulse response contains a correlation term that bounds the performance of the system, which can be avoided by using the equalizer that developed in the previous section. In this section, frequency-domain point of view of this phenomenon is studied.
The presence of the cyclic prefix (CP) greatly simplifies the equalization procedure

in OFDM-based systems. In specific, as long as the duration of channel impulse response is smaller than the length of the CP, one can use a single-tap equalizer per sub-carrier to remove the effect of the channel and recover the transmitted data symbols. Since no CP is required in FBMC systems, single-taps equalization do not fully reimburse the channel frequency selectivity through sub-carrier bands. But, if the sub-carriers number is sufficiently large, the channel frequency response becomes flat approximately over each sub-carrier band, and the equation described by (4.22) is going to be valid. So, the equalizer task can be simplified using single-tap equalization per sub-carrier.

In massive MIMO systems, it is not necessary to have a flat channel response over each sub-carrier band in order to use single tap equalizer with the channel equalizer developed previous section. In specific, even in strong frequency selective channels, the effective channel response becomes flat by using the simple single-tap per sub-carrier equalization and by incorporating a large antennas number at the BS. This property has a number of advantages including decreased sensitivity to carrier frequency offset (CFO), lowered peak-to-average power ratio (PAPR), reduced sensitivity to channel time variations within the symbol duration of FBMC and decreased latency between terminals and BS. Since there is no require for flat-fading assumption over each sub-carrier band, one can widen the sub-carrier widths.

Assume that $\underline{g}_{kk'}^{i,i}(n)$ is the high-rate equivalent channel impulse response between the transmitted symbols at sub carrier $k^{'}$ and the received ones at sub-carrier K without decimation and consider a given terminal i. The underline in $\underline{g}_{kk'}^{i,i}[n]$ is a high-rate channel and differentiate it from the decimated channel response $g_{kk'}^{i,i}(n)$ in (4.34). In the MRC case for a finite value of N, $\underline{g}_{kk'}^{i,i}(n)$ can be calculated similar to (4.34) as

$$\underline{g}_{kk'}^{ii'}(n) = \frac{1}{D_k^{i,i}} \sum_{j=0}^{N-1} (H_k^{j,i})^* (g_{k'}(m) * h_{j,i}(m) * g_k^*(-m)) \tag{4.39}$$

Applying a DTFT, we get

$$\begin{aligned} G_{kk'}^{ii}(\omega) &= \frac{1}{D_k^{i,i}} \sum_{j=0}^{N-1} (H_k^{j,i})^* G_{k'}(\omega) H_{j,i}(\omega) G_k^*(\omega) \\ &= C_k^{i,i}(\omega) G_{k'}(\omega) G_k^*(\omega) \end{aligned} \tag{4.40}$$

Where

$$C_k^{i,i}(\omega) = \frac{1}{D_k^{i,i}} \sum_{j=0}^{N-1} (H_k^{j,i})^* H_{j,i}(\omega) \tag{4.41}$$

In (4.40) given above, the two modulated square-root Nyquist filters are $G_{k'}(\omega)$ and $G_k^*(\omega)$, which implies, $Q(\omega) = |G(\omega)|^2$ is a Nyquist pulse, and $C_k^{i,i}(\omega)$ is a gain due to the multipath channel. In ideal case,the corelation $C_k^{i,i}(\omega)$ should be flat over the pass band of the sub-carrier k in order to the symbols of sub-carrier k can be perfectly reconstructed with no any interference. However, the term $C_k^{i,i}(\omega)$ may introduce some distortion over the pass band of sub-carrier k if the channel is a frequency-selective type and, as a result some interference can be occurred in the detected symbols. Using the law of large numbers, and according to (4.35), the gain $C_k^{i,i}(\omega)$ approaches to $\rho_k(\omega)$ as the number of BS antennas increases to large. Therefore, by increasing the BS array size the flat-fading condition may not be achieved.

Similarly, utilizing the equalizer in (4.38), the frequency domain of the equivalent channel can be expressed as:

$$\tilde{G}_{kk'}^{ii}(\omega) = \tilde{C}_k^{i,i}(\omega) G_{k'}(\omega) G_k^*(\omega) \tag{4.42}$$

where

$$\tilde{C}_k^{i,i}(\omega) = \frac{\sum_{j=0}^{N-1} (H_k^{j,i})^* H_{j,i}(\omega)}{D_k^{i,i} \rho_k(\omega)} = \frac{C_k^{i,i}(\omega)}{\rho_k(\omega)} \tag{4.43}$$

Therefore, $\tilde{C}_k^{i,i}(\omega)$ will approaches to a frequency flat channel due to that $C_k^{i,i}(\omega)$ asymptotically tends to $\rho_k(\omega)$. Hence, no distortion is expected in large antenna system. The massive MIMO -based FBMC systems channel flattening effect is shown in 4.5

Assuming $M = 512$ in fig. 4.5, and considering an exponentially decaying channel PDP with the decaying factor of 0.06 and the length of $L_h = 50$ for sub-carrier $k = 0$ to achieve the results. The equivalent channel becomes flat only when the channel equalizer is used with the number of BS antennas increases.

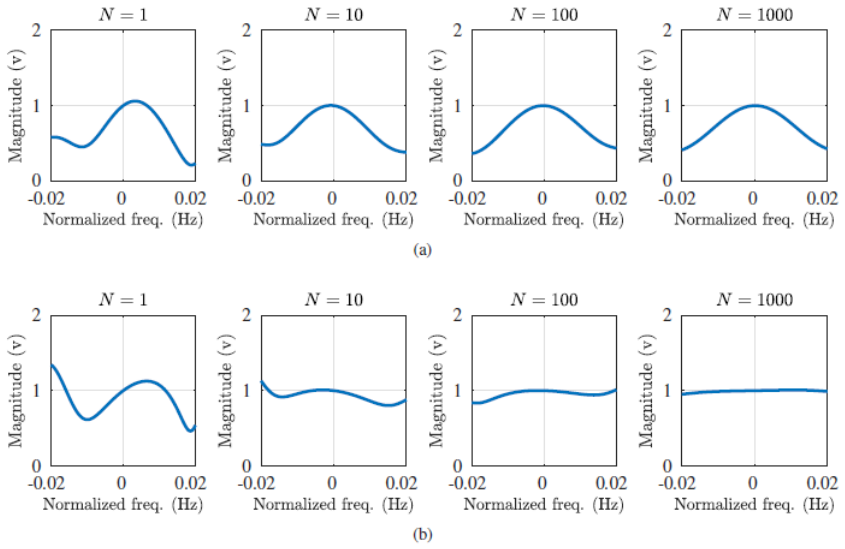

FIGURE 4.5: Equivalent channel response for different number of BS antenna,a)without channel equalizer, b)with channel equalizer

4.3.3 SINR and Achievable Rate

The SINR and channel capacity performance of an FBMC-based massive MIMO system in the uplink with the channel equalizer are analyzed in this section. The three most prominent linear combiners namely, MRC and ZF and MMSE are considered. As discussed earlier, in the large antenna system, all the linear combiners in (4.32) are approximated to $\frac{1}{N}H_k$. To analyze the system, the approach given in 4.9 is considered. The receiver filter $g_k^*(-m)$ and the equalizer $\phi_k(l)$ can be combined together as a single filtering block with impulse response $\tilde{g}_{i,k}^*(-m) = g_k^*(-m) * \phi_k[l]$ at receiver side as shown in 4.9. The modified prototype filter and the original PHYDYAS filter time and frequency responses are present in the Fig. 4.6 and 4.8, respectively. In case of time response indicated in Fig.4.6,there is a little time delay between modified and original PHYDYAS filter response.

The sinc pulse shown in Fig.4.7 and 4.8,which is the sub-carriers pulse-shape in OFDM is used as a reference. Significantly, lower spectral leakage is obtained from both prototype filters compared to the sinc pulse. In particular, the modified prototype filter has lower spectral leakage compared to original PHYDYAS filter. The modified prototype filters and original filter do not differ significantly in shape in time domain, but, there is a time delay between them, and completely they give different SINR behaviors. The new receiver filter $\tilde{g}_k^*(-m)$ can be considered in place, and to get the estimated data symbols (4.31)is used. Let assume that

$\tilde{H}^{i}_{kk',nn'}$ be an $N \times K$ matrix which has elements given by (4.29) however instead of $g^{*}_{k}(-m)$ the new filter $\tilde{g}^{*}_{i,k}(-m)$ in placed .

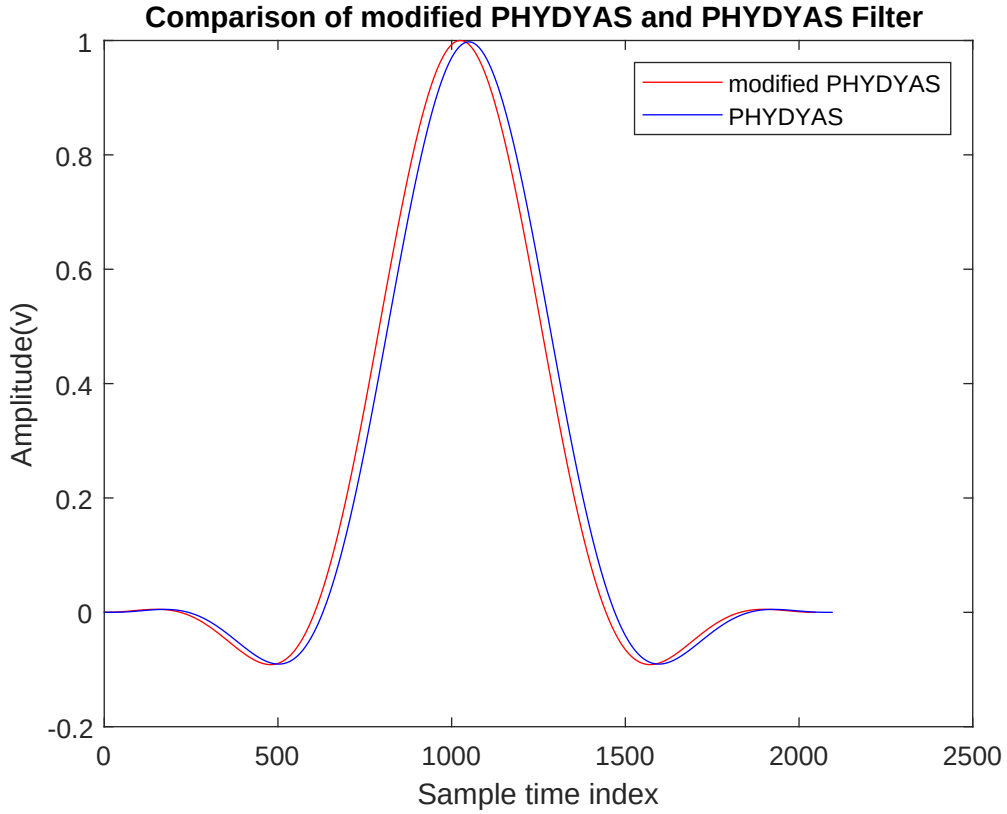

FIGURE 4.6: Impulse responses of the PHYDYAS and modified PHYDYAS filters.

Moreover, similar to $G_{kk',nn'}$, the $K \times K$ matrix $\tilde{G}_{kk',nn'}$ is formed. In specific, the $\tilde{G}_{kk',nn'}$ i^{th} row can be derived as $w^{H}_{k,i}\tilde{H}^{i}_{kk',nn'}$, where $w_{k,i}$ is the i^{th} column of the combiner matrix W_k. Therefore, the interference coefficients are calculated by the real part of the elements of $\tilde{G}_{kk',nn'}$. In order to simple SINR analysis, it is important to calculate the elements of $\tilde{G}_{kk',nn'}$ in a matrix form. In (4.44), the multi-antenna combining, convolution, phase compensation and down-sampling operations can all be expressed compactly, based on (4.29) and (4.31).

$$\tilde{G}^{i,i'}_{kk',nn'} = (\psi^{i}_{kk',nn'})^{H} g^{i,i'}_{k} \tag{4.44}$$

where

$$g^{i,i'}_{k} = \sum_{j=0}^{N-1} (W^{j,i}_{k})^{*} h_{j,i'} \tag{4.45}$$

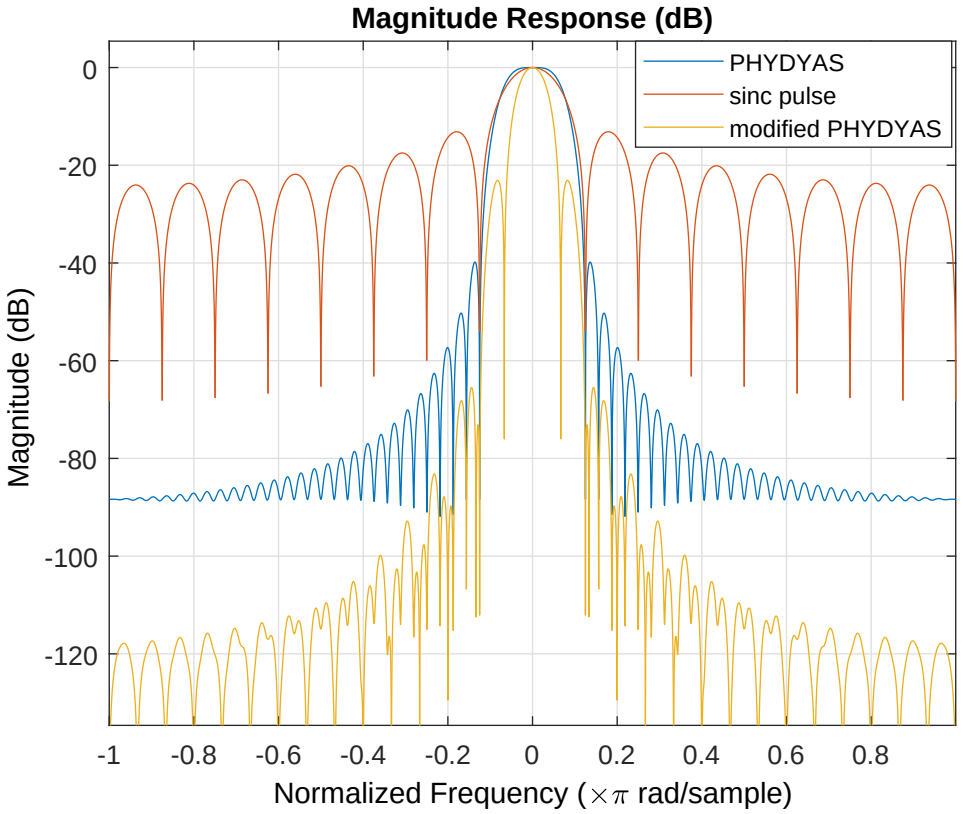

FIGURE 4.7: Frequency responses of the PHYDYAS and modified PHYDYAS filters and comparison with the sinc pulse.

and

$$(\psi^{i}_{kk',nn'})^{H} = e^{j(\phi_{k',n'}-\phi_{k,n})} e^{T}_{nn'} \tilde{G}_{i,k} G_{m'} \tag{4.46}$$

Where, $g^{i,i'}_{k}$ is the effective multi-path channel response vector between terminals i and i' at sub-carrier k, after the combining operation. $h_{j,i} = [h_{j,i}[0], ..., h_{j,i}[L_h - 1]^T$ is the channel response vector between i^{th} terminal and j^{th} BS antenna. $\tilde{G}_{i,k}$ and $G_{k'}$ are two toeplitz matrices which are defined in (4.47) and (4.48), respectively, and show the synthesis filter at sub-carrier k' and the new analysis filter at sub-carrier k, respectively. The size of the matrix $G_{k'}$ is $(L_f + L_h - 1) \times L_h$. By using (4.22) and $g_m[l] = \tilde{g}_{i,k}[l] * \rho^{*}_{k}[-l]$, we can determine the size of $\tilde{G}_{i,k}$. Thus, the new filter length $\tilde{g}_{i,k}(l)$ can be calculated as $L_{\tilde{f}} = L_f - L_h + 1$. And, the $\tilde{G}_{i,k}$ size can be obtained as $(2L_f - 1) \times (L_f + L_h - 1)$. For the down-sampling operation, the vector $e_{nn'}$ with $(2L_f - 1) \times 1$ is accounted and it contains zeros except on its $(L_f + (nn)\frac{M}{2})^{th}$ entry which is equal to one. Finally, due to the phase

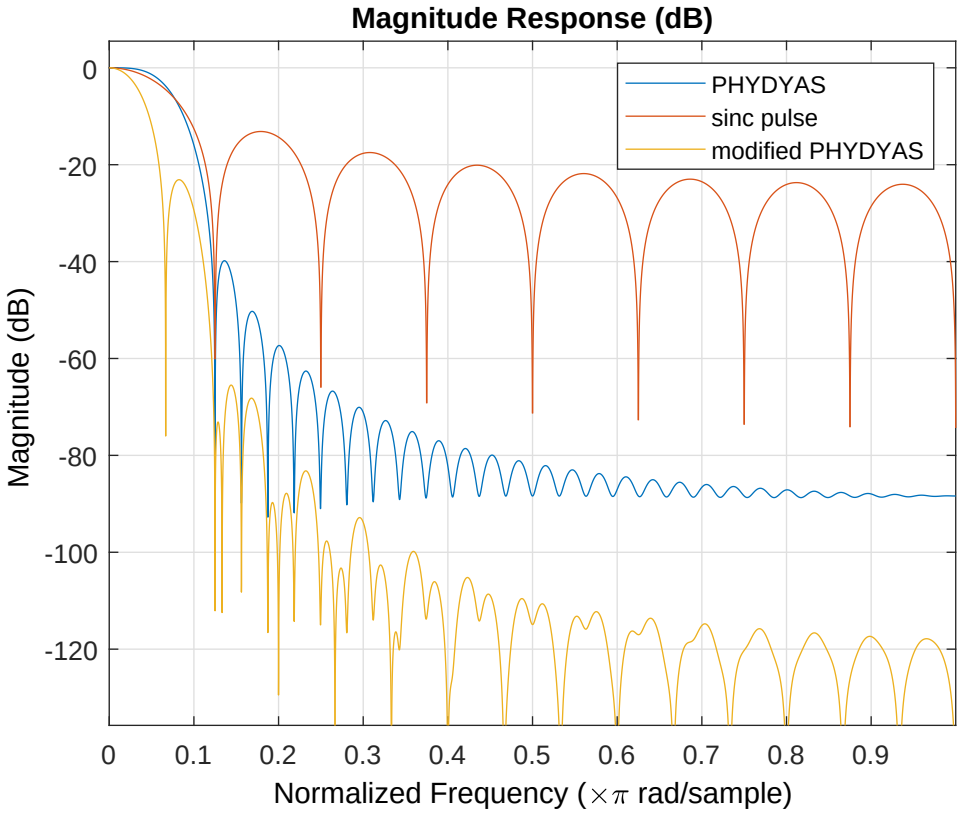

FIGURE 4.8: Frequency responses of the PHYDYAS and modified PHYDYAS filters and comparison with the sinc pulse.

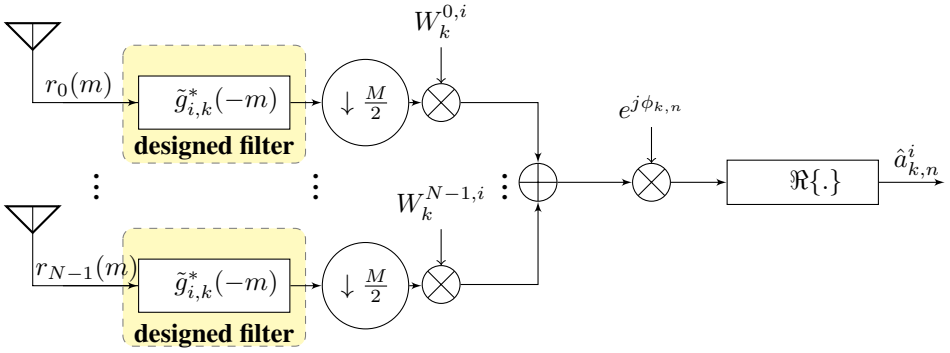

FIGURE 4.9: Block diagram of the receiver after analysis filter bank combined with channel equalizer.

compensation, $e^{j(\phi_{k',n'}-\phi_{k,n})}$ is there.

$$G_{k'} = \begin{pmatrix} g_{k'}[0] & 0 & \cdots & 0 & 0 \\ g_{k'}[1] & g_{k'}[0] & \cdots & 0 & 0 \\ \vdots & \vdots & \vdots & \vdots & \vdots \\ 0 & 0 & \cdots & g_{k'}[L_f-1] & g_{k'}[L_f-2] \\ 0 & 0 & \cdots & 0 & g_{k'}[L_f-1] \end{pmatrix} \tag{4.47}$$

$$\tilde{G}_{i,k} = \begin{pmatrix} \tilde{g}^*_{i,k}[L_{\tilde{f}}-1] & 0 & \cdots & 0 & 0 \\ \tilde{g}^*_{i,k}[L_{\tilde{f}}-2] & g_{k'}[L_{\tilde{f}}-1] & \cdots & 0 & 0 \\ \vdots & \vdots & \vdots & \vdots & \vdots \\ 0 & 0 & \cdots & \tilde{g}^*_{i,k}[1] & \tilde{g}^*_{i,k}[0] \\ 0 & 0 & \cdots & 0 & \tilde{g}^*_{i,k}[0] \end{pmatrix} \tag{4.48}$$

In (4.44), the term $\psi^i_{kk',nn'}$ is completely deterministic, and $g^{i,i'}_k$ is a random vector. Therefore, the interference coefficients are separated in to random and deterministic components in this equation. Hence, $g^{i,i'}_k$ is directly related to the combining method and can be evaluated for each combiner separately and $\psi^i_{kk',nn'}$ does not depend on the combining type.

A. MRC

D_k in (4.32) approaches to NI_K as the number of BS antennas increases larger, in MRC. And, it gives $g^{i,i'}_k = \frac{1}{N}\sum_{j=0}^{N-1}(H^{j,i}_k)^* h_{j,i'}$. The complex random vector $g^{i,i'}_k$ first and second order statistics are calculated in the Appendix. The result is

$$\mu^{i,i'}_k = E\left\{g^{i,i'}_k\right\} = \delta_{ii'}\rho_{i,k} \tag{4.49}$$

$$\Gamma^{i,i'}_k = E\left\{(g^{i,i'}_k - \mu^{i,i'}_k)(g^{i,i'}_k - \mu^{i,i'}_k)^H\right\} = \frac{1}{N}D_{\rho_{i'}} \tag{4.50}$$

$$\kappa^{i,i'}_k = E\left\{(g^{i,i'}_k - \mu^{i,i'}_k)(g^{i,i'}_k - \mu^{i,i'}_k)^T\right\} = \frac{1}{N}\delta_{ii'}\rho_{i,k}\rho^T_{i,k} \tag{4.51}$$

where $D_p = diag\left\{[\rho_k[0], \rho_k[1], ..., \rho_k[L_h-1]]^T\right\}$, and $\rho_{i,k} = [\rho_{i,k}[0], \rho_{i,k}[1], ..., \rho_{i,k}[L_h-1]]^T$. Let assume that $\gamma^{i,i'}_k$ is a zero-mean random vector which is defined as $\gamma^{i,i'}_k = (g^{i,i'}_k - \mu^{i,i'}_k)$. Thus, from (4.44) and (4.49) and resulted in

$$\begin{aligned} \tilde{G}^{i,i'}_{kk',nn'} &= (\psi^i_{kk',nn'})^H\gamma^{i,i'}_k + \delta_{ii'}(\psi^i_{kk',nn'})^H\rho_{i,k} \\ &= (\psi^i_{ii',nn'})^H\gamma^{i,i'}_k + \delta_{ii'}(\delta_{kk'}\delta_{nn'} + jA_{kk',nn'}) \end{aligned} \tag{4.52}$$

Where, $A_{kk',nn'} = \Im\{\sum_{m=-\infty}^{+\infty} g_{k',n'}[m]g^*_{k,n}[m]\}$. the fact that $e^{j(\phi_{k',n'}-\phi_{k,n})}e^T_{nn'}\tilde{G}_{i,k}G_{m'} = \delta_{kk'}\delta_{nn'} + jA_{kk',nn'}$ is used to get the second line of (4.52). This result is obtained from FBMC the real-orthogonality property given in (4.9), and the fact that the

modulated channel PDP effect is removed by $\rho_k[l]$ the equalizer $\phi_k[l]$. As discussed above, the real part of $\tilde{G}_{kk',nn'}$ elements represent the interference coefficients. Assume $R_{kk',nn'} = \Re\left\{\tilde{G}_{kk',nn'}\right\}$, and $\gamma''_{k,n} = \Re\left\{\gamma'_{k,n}\right\}$. Then, (4.31) can be rearranged as:

$$\hat{a}_{k,n} = \sum_{n'=-\infty}^{+\infty} \sum_{k'=0}^{M-1} R_{kk',nn'} a_{k',n'} + \gamma''_{k,n} \tag{4.53}$$

An expression for the elements of $R_{kk',nn'}$ can be obtained by decomposing the matrices and vectors in to the real and imaginary parts which constitute the elements of $\tilde{G}_{kk',nn'}$, . Specifically, $\breve{a} = \left[\Re\left\{a^T\right\}, \Im\left\{a^T\right\}\right]^T$ is defined for an arbitrary complex vector or matrix a. Therefore, the elements of $R_{kk',nn'}$ can be obtained from (4.52) as:

$$R^{i,i'}_{kk',nn'} = (\breve{\psi}^i_{kk',nn'})^T \breve{\gamma}^{i,i'}_k + \delta_{ii'}\delta_{kk'}\delta_{nn'} \tag{4.54}$$

Where, $\breve{\gamma}^{i,i'}_k$ is the real-valued random vector which has zero-mean and using ((4.49), (4.50), (4.51)) its covariance matrix can be calculated as:

$$\begin{aligned} C^{i,i'}_k &= E\left\{\left(\breve{\gamma}^{i,i'}_k - E\left\{\breve{\gamma}^{i,i'}_k\right\}\right)\left(\breve{\gamma}^{i,i'}_k - E\left\{\breve{\gamma}^{i,i'}_k\right\}\right)^T\right\} \\ &= \frac{1}{2}\begin{bmatrix} \Re\{\Gamma^{i,i'}_k + \kappa^{i,i'}_k\} & \Im\{-\Gamma^{i,i'}_k + \kappa^{i,i'}_k\} \\ \Im\{\Gamma^{i,i'}_k + \kappa^{i,i'}_k\} & \Re\{\Gamma^{i,i'}_k - \kappa^{i,i'}_k\} \end{bmatrix} \\ &= \frac{1}{N}(\bar{D}_{\rho_{k'}} + \delta_{ii'}\bar{\rho}_{i,k}) \end{aligned} \tag{4.55}$$

where $\bar{D}_{\rho_{k'}} = \frac{1}{2}\begin{bmatrix} D_{\rho_{i'}} & 0 \\ 0 & D_{\rho_{i'}} \end{bmatrix}$ and $\bar{\rho}_{i,k} = \frac{1}{2}\begin{bmatrix} \Re\{\rho_{i,k}\rho^T_{i,k}\} & \Im\{\rho_{i,k}\rho^T_{i,k}\} \\ \Im\{\rho_{i,k}\rho^T_{i,k}\} & -\Re\{\rho_{i,k}\rho^T_{i,k}\} \end{bmatrix}$

The instantaneous power corresponding to $R^{i,i'}_{kk',nn'}$ can be determined as $P^{i,i'}_{kk',nn'} = \left(R^{i,i'}_{kk',nn'}\right)^2 = (\breve{\gamma}^{i,i'}_k)^T \Psi^i_{kk',nn'} \breve{\gamma}^{i,i'}_k + \delta_{ii'}\delta_{kk'}\delta_{nn'} + 2\delta_{ii'}\delta_{kk'}\delta_{nn'}(\breve{\psi}^i_{kk',nn'})^T \breve{\gamma}^{i,i'}_k$ where, $\Psi^i_{kk',nn'} = \breve{\psi}^i_{kk',nn'}(\breve{\psi}^i_{kk',nn'})^T$ from (4.54). The average power over different channel realizations can be derived using the concept of moment of quadratic form in the non-singular normal case and from above equation [[63], p. 53].

$$\begin{aligned} \bar{P}^{i,i'}_{kk',nn'} &= tr\{C^{i,i'}_k \Psi^i_{kk',nn'}\} + \delta_{ii'}\delta_{kk'}\delta_{nn'} \\ &= \frac{1}{N} tr(\bar{D}_{\rho_{k'}} + \delta_{ii'}\bar{\rho}_{i,k})\Psi^i_{kk',nn'} + \delta_{ii'}\delta_{kk'}\delta_{nn'} \end{aligned} \tag{4.56}$$

With the channel equalizer and MRC combiner, SINR can be calculated using (4.57) in the uplink of the FBMC massive MIMO system.

$$
\begin{aligned}
SINR_{k,n}^{i} &= \frac{\bar{P}_{kk',nn'}^{i,i'}}{\sum_{n'=-\infty}^{+\infty}\sum_{k'=0}^{M-1}\bar{P}_{kk',nn'}^{i,i'} + \sum_{n'=-\infty}^{+\infty}\sum_{k'=0}^{M-1}\sum_{\substack{i'=0\\ i'\neq i}}^{K-1}\bar{P}_{kk',nn'}^{i,i'} + \sigma^2} \\
&= \frac{N + tr\{(\bar{D}_{\rho_{k'}} + \bar{\rho}_{i,k})\Psi_{kk',nn'}^{i}\}}{\sum_{\substack{i'=0\\ i'\neq i}}^{K-1}\sum_{n'=-\infty}^{+\infty}\sum_{k'=0}^{M-1} tr\{\bar{D}_{\rho_{k'}}\Psi_{kk',nn'}^{i}\} + \sum_{\substack{n'=-\infty\\ (k',n')\neq (k,n)}}^{+\infty}\sum_{k'=0}^{M-1} tr\{(\bar{D}_{\rho_{k'}} + \bar{\rho}_{i,k})\Psi_{kk',nn'}^{i}\} + \sigma^2}
\end{aligned}
\tag{4.57}
$$

The SINR in (4.37) that is without the channel equalizer and MRC combiner is approximated to (4.58) for large number of base station N

$$
SINR_{k,n}^{i^{MRC}} \approx \frac{(N+1)\tau}{(K-1)\tau + \sigma_{\gamma}^{2}} \tag{4.58}
$$

where $\tau = |\rho_{i,k}|^2$.

Achievable Rate

In the uplink of an FBMC massive MIMO system with the channel equalizer and MRC combiner, achievable rate can be calculated or derived from SINR for each user at the output of the MRC combiner as follow

$$
R_{i}^{MRC-weq} = log2\big(1 + SINR_{k,n}^{i}\big) \tag{4.59}
$$

And for conventional MRC, the achievable rate can be calculated or derived from (4.58) for each user at the output of the MRC combiner as follow,

$$
R_{i}^{MRC} = log_2\Big(1 + SINR_{k,n}^{i^{MRC}}\Big) \approx log_2\Big(1 + \frac{(N+1)\tau}{(K-1)\tau + \sigma_{\gamma}^{2}}\Big) \tag{4.60}
$$

Spectral Efficiency

Spectral Efficiency refers to achievable data rate over a given bandwidth in a specific wireless communication system.

B. ZF

In the uplink, the FBMC massive MIMO system with the channel equalizer with ZF combiner, and provided that $N \geq K+1$, SINR can be determined in (4.65). This can be determined from the covariance matrix given in (4.64) and the random vector g_k^{i,i^i} first and second order statistics can be determined as given below and its proof is given in the appendix.

$$\mu_k^{i,i'} = = \delta_{ii'}\rho_{i,k} \tag{4.61}$$

$$\Gamma_k^{i,i'} = = \frac{1}{N-K}(D_{\rho_{i'}} - \rho_{i',k}\rho_{i',k}^H) \tag{4.62}$$

$$\kappa_k^{i,i'} = 0 \tag{4.63}$$

Hence, the covariance matrix of $\check{\gamma}_k^{i,i'}$ is calculated by

$$C_k^{i,i'} = \frac{1}{N-K}(\bar{D}_{\rho_{k'}} + \bar{\rho}_{i,k}) \tag{4.64}$$

Where, $\bar{\rho}_{i,k} = \frac{1}{2}\begin{bmatrix} \Re\{\rho_{i,k}\rho_{i,k}^H\} & -\Im\{\rho_{i,k}\rho_{i,k}^H\} \\ \Im\{\rho_{i,k}\rho_{i,k}^H\} & \Re\{\rho_{i,k}\rho_{i,k}^H\} \end{bmatrix}$

$$SINR_{k,n}^i = \frac{N-K}{\sum_{i'=0}^{K-1}\sum_{\substack{n'=-\infty \\ (k',n')\neq}}^{+\infty}\sum_{\substack{k'=0 \\ (k,n)}}^{M-1} tr\{(\bar{D}_{\rho_{k'}} - \bar{\rho}_{i,k})\Psi_{kk',nn'}^i\} + \sigma_\gamma^2} \tag{4.65}$$

The SINR in (4.37) that is without the channel equalizer and for ZF detectors is approximated to (4.66) for large number of base station N

$$SINR_{k,n}^{i^{ZF}} \approx \frac{(N-K)\tau}{\sigma_\gamma^2} \tag{4.66}$$

Achievable Rate

In the uplink, FBMC massive MIMO system with the channel equalizer using ZF combiner, and provided that $N \geq K+1$, achievable rate can be calculated or derived from SINR for each user at the output of the ZF combiner as follow

$$R_i^{ZF-weq} = log_2\{(1 + SINR_{k,n}^i)\} \tag{4.67}$$

And without channel equalizer, the achievable rate can be calculated or derived from (4.66) for each user at the output of the ZF detector as follow,

$$R_i^{ZF} = log_2\Big(1 + SINR_{k,n}^{i^{ZF}}\Big) \approx log2\bigg(1 + \frac{(N-K)\tau}{\sigma_\gamma^2}\bigg) \tag{4.68}$$

Note that the performance of the Minimum Mean-Square Error (MMSE)is done through matlab simulation only in this paper.

4.3.4 Computational complexity FBMC System

Despite several advantages, FBMC is more computationally complex than conventional OFDM. The computational complexity of any multicarrier scheme can be evaluated by calculating the number of real multiplications involved in computing a length-N complex-valued output sequence. In OFDM, the computational complexity comes from the IFFT and FFT operations and its complexity can be written as [[34], pp. 23]

$$C_{OFDM} = 2 \times [Nlog2N \times 3N + 4] \tag{4.69}$$

The computational complexity of FBMC can be evaluated by calculating the real multiplications involved in SFB at the transmitter and AFB at the receiver. From [[34], pp. 23], the complexity of the conventional FBMC system can be written as follows

$$C_{FBMC} = 4 \times [2N + Nlog2N - 3N + 4 + 2ON] \tag{4.70}$$

But in the case of the system with equalizer, at receiver side, the receiver filter $g_k^*(-m)$ and the equalizer $\phi_k(l)$ can be combined together as a single filtering block with impulse response $\tilde{g}_{i,k}^*(-m) = g_k^*(-m) * \phi_k[l]$ as shown in 4.9. Hence, the length of the new filter $\tilde{f}_{i,k}(l)$ can be obtained as $L_{\tilde{f}} = L_f - L_h + 1 = KN - L_h + 1$.

The computational complexity of proposed FBMC system can be evaluated by calculating the real multiplications involved in the synthesis filter bank (SFB) at the transmitter (the same with that of conventional system)and analysis filter bank (AFB) at the receiver using the new filter $\tilde{f}_{i,k}(l)$. The computational complexity of the FBMC System with channel equalizer reduced by the factor of $8L_h$ compared with conventional FBMC System. The real multiplications involved in linear combiners are not included in the computational complexity of both system

because their effect for both system are the same.

$$C^*_{FBMC} = 4 \times [2N + Nlog2N - 3N + 4 + 2ON - 2L_h], \tag{4.71}$$

Where, C^*_{FBMC} is the computational complexity of the FBMC System with channel equalizer.

Chapter 5

Result and Discussion

The previous sections analysis are evaluated using computer simulations for both systems and presented in this section. The PHYDYAS prototype filter is used at terminals to synthesize and analyze their FBMC signals with overlapping factor of 4. The assumptions used in this simulation are number of sub-carriers M = 1024, number of terminals K = 10 and the selected noise level is such that the SNR at the BS antennas input is fixed to 15 dB. Additionally, for different terminals with multi-path length $L_h = 40$, the normalized exponentially decaying channel PDP, $\rho(l) = e^{(-\alpha l)} / \left(\sum_{l=0}^{L-1} e^{(-\alpha l)}\right) l = 0, 1, ..., L-1$ for $k = 0, ..., K-1$ with different decaying factors $\alpha_k = (k+1)/20$ is used and bandwidth = 10MHz which equal with sampling frequency is considered.

Using above assumptions, the FBMC massive MIMO system with and without channel equalizer is developed using code and the results are obtained as given below. Then, the performance analysis of the system with and without equalizer is done based on the results. The SINR with and without the channel is compared at the BS(receiver)and presented in Fig. 5.1. That means, the performance of average SINR of MRC, ZF, and MMSE detectos as a function of different number of BS antennas over different channel realizations is done for both systems. The SINR performance of MRC, ZF, and MMSE detectors without channel equalizer approach to the saturation level predicted by (4.37) as N increases to large as shown in the Fig. 5.1. That mean by increasing the BS antennas number, arbitrarily large SINR values cannot be obtained.

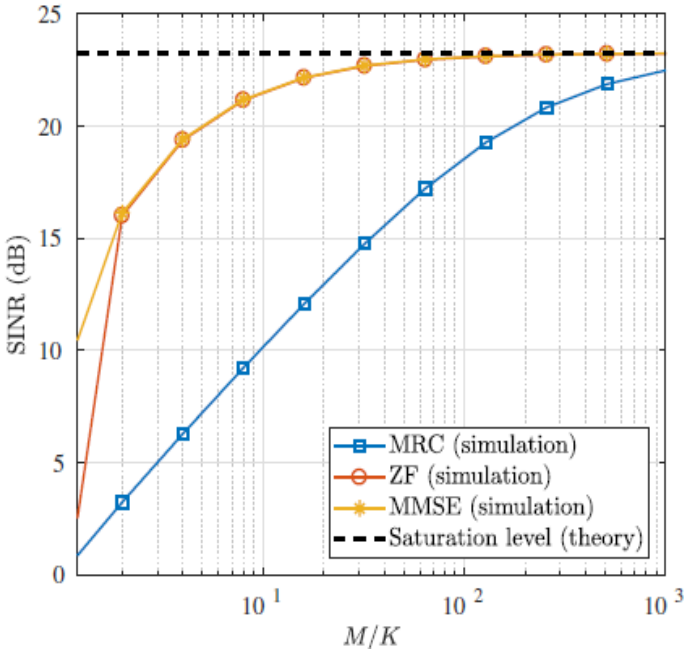

FIGURE 5.1: SINR performance comparison for the case that the proposed equalizer is not used

However, the performance of FBMC with the channel equalizer in place the saturation problem is avoided as shown in Fig. 5.2. This figure shows the SINR performance of MRC, ZF, and MMSE detectors as a function of different number of BS antennas. Using the modified prototype filter, the saturation problem of the conventional FBMC systems in massive MIMO channels is avoided and arbitrarily large SINR values can be achieved by increasing N. The theoretical SINR values for MRC, combiners with and without equalizer are presented, as calculated in (4.58),(4.57), (4.66) and (4.65). in particular, ZF and MMSE detectors give better improvement(around 17dB per-user for ZF and MMSE, and 2dB per-user for MRC) than MRC detector.

The achievable rate with and without the equalizer is conducted in Fig. 5.3. This figure shows the FBMC massive MIMO system achievable rate simulation of MRC, ZF and MMSE detectors with and without channel equalizer. As shown in Figs. 5.3, in FBMC massive MIMO system with modified prototype filter, higher spectral efficiency is achieved compared to FBMC massive MIMO system with original prototype filter for all linear detectors. In particular, the achievable rate or Spectral efficiency of the system increases by 6 bits per second per hertz for ZF

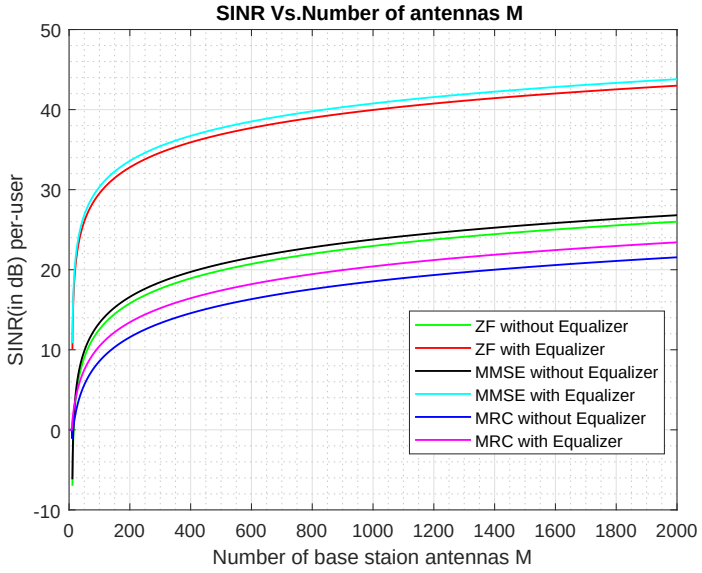

FIGURE 5.2: SINR performance comparison for modified prototype filter and existing one .

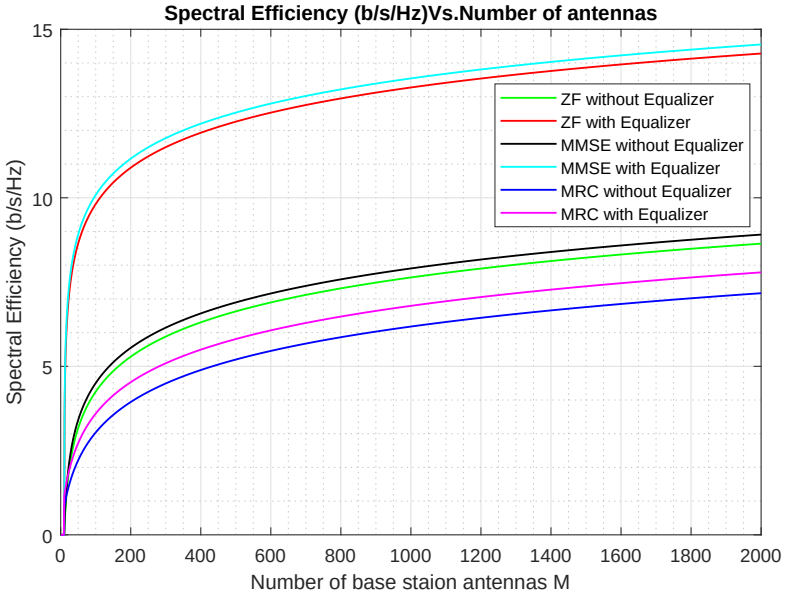

FIGURE 5.3: Spectral Efficiency performance comparison for modified prototype filter and existing one .

and MMSE, and 1 bits per second per hertz for MRC.

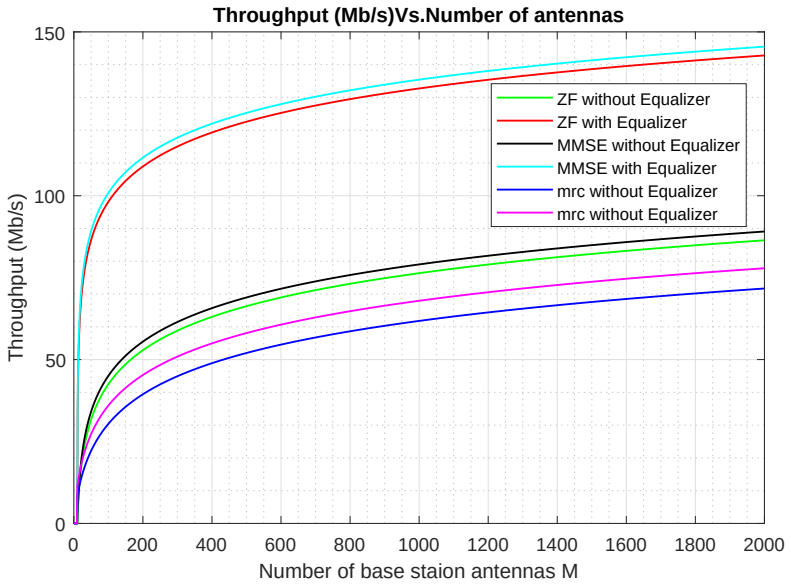

FIGURE 5.4: Throughput performance comparison for modified prototype filter and existing one .

As shown in Figs. 5.4, in FBMC system with modified prototype filter, higher throughout is obtained compared to FBMC system with conventional prototype filter for all linear detectors in the massive MIMO system. specifically, the throughput increased by 54 megabits per second for ZF and MMSE and and 8 megabits per second for MRC when we compare both system. Hence, as expected, by eliminating the correlation between the multi-antenna combining tap values and the channel impulse responses between the mobile terminals and the BS antennas we can achieve a higher spectral efficiency and throughout compared with the conventional FBMC systems in the Massive MIMO systems.

In Fig. 5.5, we compare the BER of the conventional prototype filter and modified prototype filter that of FBMC with ZF. In BER simulations, we consider offset 16-QAM modulation, K = 10 users and M = 200 BS antennas. Based on our results,ZF with modified prototype filter has higher BER performance compared to conventional prototype filter. That means the conventional ZF has a poor performance compared to proposed one. And also based on 5.5 , the conventional MRC has a poor BER performance compared to MRC with equalizer.
By using new design prototype filter, the computational complexity of the FBMC system reduced when we compare with conventional FBMC system as shown in Fig. 5.6. In another word, the cost of the system is minimized because it is directly proportional to computational complexity of the system.

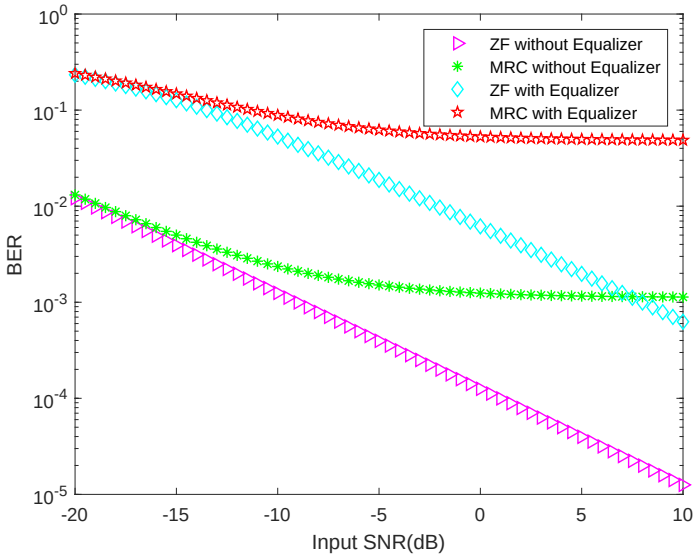

FIGURE 5.5: Bit Error Rate performance comparison for modified prototype filter and existing one .

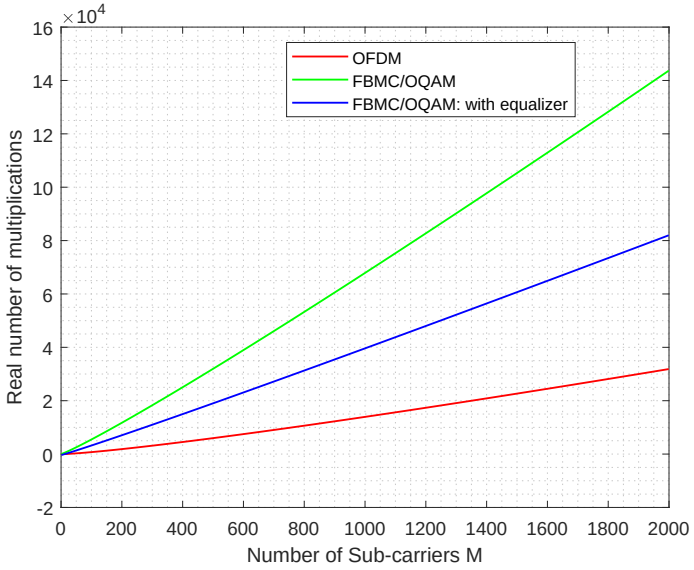

FIGURE 5.6: Computational complexity FBMC System

Chapter 6

Conclusions and Future works

6.1 Conclusions

In this thesis, the channel capacity improvement of FBMC transmission in the context of massive MIMO is studied by considering single-tap-per-subcarrier equalization using the conventional linear combiners, i.e., MRC,and ZF. The correlation between the multi-antenna combining tap weights and the channel impulse responses leads to an interference which does not fade away even with an infinite number of BS antennas. Hence, arbitrarily large SINR and channel capacity values cannot be achieved. Moreover, spectral efficiency and throughput are not effectively increase. By identifying the source of SINR saturation and limitation of increment of channel capacity, upper bounded SINR and asymptotic achievable information rate are derived. An efficient equalization method is proposed to remove this correlation and to resolve the problem. Mathematically, the performance of the FBMC system that incorporating the proposed equalization method is analyzed and closed-form expressions for the SINR and the asymptotic achievable information rate of the proposed receiver design in the cases of MRC and ZF are derived. Computational complexity of FBMC system is done using proposed method and it is reduced. Finally, by removing the correlation using the proposed technique, a higher spectral efficiency and throughput, and a Lower BER are obtained compared to the conventional FBMC-based massive MIMO systems.

6.2 Future works

This thesis has addressed the issue of the association of FBMC modulation to Massive MIMO systems. A number of interesting topics, based on the research issues studied in this thesis, could also be addressed. But, There is potential for further research in the areas discussed here and as well as related areas.

- to make the system simple, the proposed method is done using the assumption that CSI is fully known at the receiver side. It would be of interest to study the influence of channel estimation errors on the performance of the proposed receivers, and adapt them to more realistic conditions.
- In chapter 4, Although the proposed method resolves the saturation problem, it may not be of practical interest as it may lead to a very complex receiver. The source of the complexity lies in the requirement of a separate filter $\phi_k[l]$ per user per antenna. Hence, the receiver front-end processing has to be repeated for each terminal separately.

Appendix

THE $g_k^{i,i'}$ STATISTICS CALCULATION

A. MRC

For MRC, $g_k^{ii'} = \frac{1}{D_k^{i,i}} \sum_{j=0}^{N-1} (H_k^{j,i})^* h_{j,i'}$ is there. Moreover, due to the law of large numbers,$D_k^{i,i}$ approaches to N for N large values. Hence, the$g_k^{i,i'}$ element l^{th} mean, for $l \in 0, ..., L_h - 1$, can be determined as follows:

$$\begin{aligned} E\{g_k^{i,i'}[l]\} &= \frac{1}{N} \sum_{j=0}^{N-1} \sum_{l=0}^{L_h-1} E\left\{h_{j,i}^*[l] h_{j,i'}[l)\right\} e^{j2\pi \frac{kl}{M}} \\ &= \rho(l) e^{j2\pi \frac{kl}{M}} \delta_{ii'} = \delta_{ii'} \rho_{i,k}(l) \end{aligned} \tag{6.1}$$

This gives (4.49). Then, the correlation between $g_k^{i,i'}[l]$ and $g_k^{i,i'}[l']$ for $l, l' \in 0, ..., L_h - 1$ can be calculated. The case that $i \neq i'$ is considered. Hence,

$$\begin{aligned} E\{g_k^{i,i'}[l](g_k^{i,i'}[l'])^*\} &= \frac{1}{N^2} \sum_{j=0}^{N-1} \sum_{i'=0}^{N-1} E\left\{(H_k^{j,i})^* H_k^{j',i} h_{j,i'}[l] h_{j',i'}^*[l']\right\} \\ &= \frac{1}{N^2} \sum_{j=0}^{N-1} \sum_{i'=0}^{N-1} \sum_{l=0}^{L_h-1} \sum_{l'=0}^{L_h-1} E\left\{(h_{j,i})^*[l] h_{j',i}[l'] h_{j,i'}[l] h_{j',i'}^*[l']\right\} \\ &\quad \times e^{j2\pi \frac{k(l-l')}{M}} = \frac{1}{N} \delta_{ll'} \rho_{i'}(l), \qquad for \;\; i \neq i' \end{aligned}$$

The co-variance matrix $\Gamma_k^{i,i^{'}}$ given in (4.50) can be calculated from the correlation which can be calculated as follow for the $i \neq i^{'}$ case.

$$\begin{aligned} E\{g_k^{i,i}[l](g_k^{i,i}[l^{'}])^*\} &= \frac{1}{N^2}\sum_{j=0}^{N-1}\sum_{i^{'}=0}^{N-1} E\left\{(H_k^{j,i})^* H_k^{j^{'},i} h_{j,i}[l] h_{j^{'},i}^*[l^{'}]\right\} \\ &= \frac{1}{N^2}\sum_{j=0}^{N-1}\sum_{i^{'}=0}^{N-1}\sum_{l=0}^{L_h-1}\sum_{l^{'}=0}^{L_h-1} E\left\{(h_{j,i})^*[l] h_{j^{'},i}[l^{'}] h_{j,i}[l] h_{j^{'},i}^*[l^{'}]\right\} \\ &\quad \times e^{j2\pi\frac{k(l-l^{'})}{M}} = \frac{1}{N}\delta_{ll^{'}}\rho_{i^{'}}(l) + \rho_{i,k}(l)\rho_{i,k}^*(l^{'}) \end{aligned}$$

The pseudo-co-variance matrix $\kappa_k^{i,i^{'}}$ in (4.51) can be calculated using similar derivations line as given above.

$$\begin{aligned} E\{g_k^{i,i}[l](g_k^{i,i}[l^{'}])^T\} &= \frac{1}{N^2}\sum_{j=0}^{N-1}\sum_{i^{'}=0}^{N-1} E\left\{(H_k^{j,i})^T H_k^{j^{'},i} h_{j,i}[l] h_{j^{'},i}^T[l^{'}]\right\} \\ &= \frac{1}{N^2}\sum_{j=0}^{N-1}\sum_{i^{'}=0}^{N-1}\sum_{l=0}^{L_h-1}\sum_{l^{'}=0}^{L_h-1} E\left\{(h_{j,i})^T[l] h_{j^{'},i}[l^{'}] h_{j,i}[l] h_{j^{'},i}^T[l^{'}]\right\} \\ &\quad \times e^{j2\pi\frac{k(l+l^{'})}{M}} = \frac{1}{N}\delta_{ii^{'}}\rho_{i,k}(l)\rho_{i,k}^T(l^{'}) + \rho_{i,k}(l)\rho_{i,k}^T(l^{'}) \end{aligned}$$

B.ZF

To calculate the $g_k^{i,i^{'}}$ element $\mu_k^{i,i^{'}}$ mean in (4.61), $g_k^{i,i^{'}} = w_{k,i}^H h_{i^{'}}[\ell]$ is there, where $w_{k,i}^H$ is the combiner matrix W_k i^{th} column, $h_{i^{'}}[l]$ is an $N \times 1$ vector with its j^{th} element equal to $h_{j,i}^{'}[\ell]$, $h_{k,i}$ is the H_k i^{th} column. For ZF combiner, $W_k = H_k(H_k^H H_k)^{-1}$ is there. Hence, the $g_k^{i,i^{'}}[l]$ mean can be calculated as:

$$\begin{aligned} E\{g_k^{i,i^{'}}[\ell]\} &= E\{w_{k,i}^H h_{i^{'}}[\ell]\} \\ &= \frac{1}{M}\sum_{k=0}^{M-1} E\left\{w_{k,i}^H h_{k^{'},i^{'}}\right\} e^{j2\pi\frac{k^{'}\ell}{M}} \\ &= \frac{1}{M}\sum_{k=0}^{M-1}\sum_{l=0}^{L_h-1} E\left\{w_{k,i}^H h_{k,i^{'}}\right\}\rho_{i^{'},k}[l] e^{j2\pi\frac{k^{'}(\ell-l)}{M}} \\ &= \frac{1}{M}\sum_{k=0}^{M-1}\sum_{l=0}^{L_h-1}\delta_{ii^{'}}\rho_{i^{'},k}[l] e^{j2\pi\frac{k^{'}(\ell-l)}{M}} \\ &= \delta_{ii^{'}}\rho_{i,k}(\ell) \end{aligned}$$

The $h_{k',i'}$ of channel frequency response can be defined as a term that is correlated with $h_{k,i'}$ and a term that is $h_{k,i'}$ independent combination, i.e.,

$$h_{k',i'} = \alpha_{kk',i'} h_{k,i'} + h^{indep}_{kk',i'}, \tag{6.2}$$

where $h^{indep}_{kk',i'}$ is $h_{k,i'}$ independent and the $\alpha_{kk',i'}$ of correlation coefficient can be calculated as:

$$\alpha_{kk',i'} = E\{H^{j,i'}_{k'}(H^{j,i'}_{k})^*\} = \rho_{i'}[k' - k],$$

where $\rho_i[k] = \sum_{l=0}^{L_h} \rho_i[l] e^{-j\frac{2\pi kl}{M}}$ is the channel PDP $\rho_i[l]$ the M-point discrete Fourier transform k^{th} coefficient. For ZF combiner, a $w^H_{k,i} h_{k,i'} = \delta_{ii'}$ is there, that comes from $W_k H_k = I_i$.
Then, the correlation between $g^{i,i'}_k[\ell]$ and $g^{i,i'}_k[\ell']$ is calculated, in order to determine the co-variance matrix $\Gamma^{i,i'}_k$ in (4.62), for $\ell, \ell' \in 0, ..., L_h - 1$. And, equation (6.3) is obtained as follows:

$$\begin{aligned}
E\{g^{i,i'}_k[\ell]\left(g^{i,i'}_k[\ell']\right)^*\} &= E\{w^H_{k,i} h_{i'}[\ell] h^H_{i'}[\ell'] w_{k,i}\} \\
&= \delta_{ii'}\rho_{i,k}[\ell]\rho^*_{i,k}[\ell'] + \frac{1}{M^2}\sum_{k'=0}^{M-1}\sum_{m''=0}^{M-1} E\{w^H_{k,i} h^{indep}_{kk',i'} (h^{indep}_{kk'',i'})^H w_{k,i}\} e^{j\frac{2\pi k' \ell}{M}} \\
&\quad \times e^{-j\frac{2\pi k'' \ell'}{M}} \\
&= \delta_{ii'}\rho_{i,k}[\ell]\rho^*_{i,k}[\ell'] + \frac{1}{M^2(N-K)}\sum_{k'=0}^{M-1}\sum_{m''=0}^{M-1} \\
&\quad \left(\rho_{i'}[k' - k''] - \rho_{i'}[k' - k]\rho_{i'}[k - k'']\right) e^{j\frac{2\pi(k' \ell - k'' \ell')}{M}} \\
&= \delta_{ii'}\rho_{i,k}[\ell]\rho^*_{i,k}[\ell'] + \frac{1}{N-K}\left(\delta_{\ell\ell'}\rho_{i'}[\ell] - \rho_{i',k}[\ell]\rho^*_{i',k}[\ell']\right).
\end{aligned}$$

This comes from proof in (6.2) and from the $w_{k,i}$ independence from $h^{indep}_{kk',i'}$ and $h^{indep}_{kk'',i'}$, the correlation

$$E\left\{h^{indep}_{kk',i'}(h^{indep}_{kk'',i'})^H\right\} = \left(\rho_{i'}[k' - k''] - \rho_{i'}[k' - k]\rho_{i'}[k - k'']\right) I_N,$$

and $H^H_k H_k$ is a $K \times K$ complex central Wishart matrix with N degrees of freedom and covariance I_K, and for $N \geq K + 1$,

$$E\left[\left\{\left(W^H_k W_k\right)^{-1}\right\}\right] = E\left[\left\{\left(H^H_k H_k\right)^{-1}\right\}\right] = \frac{K}{N-K}$$

Bibliography

[1] H. Atarashi, N. Maeda, S. Abeta, and M. Sawahashi, Broadband packet wireless access based on VSF-OFCDM and MC/DS-CDMA, in Personal, Indoor and Mobile Radio Communications, 2002. The 13th IEEE International Symposium on, sept.2002, vol. 3, pp. 992 997 vol.3.

[2] K. Fazel and S. Kaiser, Multi-Carrier and Spread Spectrum Systems: From OFDM and MC-CDMA to LTE and WiMax, John Wiley and Sons, 2009.

[3] K. Etemad and M.-Y. Lai, WiMAX Technology and Network Evolution, John Wiley, 2011.

[4] WiMax Forum, Mobile System Profile, release 1.0 approved specification, Revision 1.5.0, Nov. 2007.

[5] 3GPP TS 36.211, Evolved Universal Terrestrial Radio Access (E-UTRA); Physical Channels and Modulation (Release 8).

[6] J.G.Andrews, S.Buzzi, W.Choi, S. V.Hanly, A.Lozano, A. C.Soong, et al. (2014). What will 5g be? IEEE Journal on Selected Areas in Communications, 32(6), 1065-1082.

[7] T. L. Marzetta, Noncooperative cellular wireless with unlimited numbers of base station antennas, IEEE Transactions on Wireless Communications, vol. 9, no. 11, pp. 3590-3600, 2010.

[8] D.Qiao, Y.Wu and Y.Chen (2014). Massive mimo architecture for 5g networks: Co-located, or distributed?. In: 2014 11th international symposium on wireless communications systems (ISWCS). IEEE, pp. 192-197.

[9] F.Boccardi, R. W.Heath, A.Lozano, T. L.Marzetta and P.Popovski (2014). Five disruptive technology directions for 5g. IEEE Communications Magazine, 52(2), 74-80.

[10] M. Iwamura, K. Etemad, M.-H. Fong, R. Nory, and R. Love, Carrier aggregation framework in 3GPP LTE-advanced [WiMAX/LTE update], IEEE Communications Magazine, vol. 48, no. 8, pp. 60-67, 2010.

[11] P. Banelli, S. Buzzi, G. Colavolpe, A. Modenini, F. Rusek, and A. Ugolini, Modulation formats and waveforms for 5G networks: Who will be the heir of OFDM?: An overview of alternative modulation schemes for improved spectral efficiency, IEEE Signal Processing Magazine, vol. 31, no. 6, pp. 80-93, 2014.

[12] B. Farhang-Boroujeny and H. Moradi, OFDM inspired waveforms for 5G, IEEE Communications Surveys and Tutorials, 2016.

[13] F. Schaich and T. Wild, Waveform contenders for 5G - OFDM vs. FBMC vs. UFMC, in IEEE ISCCSP 2014.

[14] A. Farhang, N. Marchetti, F. Figueiredo, and J. P. Miranda, Massive MIMO and waveform design for 5th generation wireless communication systems, in IEEE 5GU, 2014.

[15] B. Farhang-Boroujeny, OFDM versus filter bank multicarrier, IEEE Signal Processing Magazine, vol. 28, no. 3, pp. 92-112, 2011.

[16] A. Aminjavaheri, A. Farhang, A. RezazadehReyhani, and B. Farhang- Boroujeny, Impact of timing and frequency offsets on multicarrier waveform candidates for 5G, in IEEE SP/SPE 2015.

[17] A. I. Perez-Neira, M. Caus, R. Zakaria, D. Le Ruyet, E. Kofidis, M. Haardt, X. Mestre, and Y. Cheng, MIMO signal processing in offset-QAM based filter bank multicarrier systems, IEEE Transactions on Signal Processing, vol. 64, no. 21, pp. 5733-5762, 2015.

[18] A. Farhang, N. Marchetti, L. E. Doyle, and B. Farhang-Boroujeny, Filter bank multicarrier for massive MIMO, in 2014 IEEE 80th Vehicular Technology Conference (VTC2014-Fall), pp. 1-7, 2014.

[19] A. Aminjavaheri, A. Farhang, N. Marchetti, L. E. Doyle, and B. Farhang-Boroujeny, Frequency spreading equalization in multicarrier massive MIMO, in IEEE ICC, 2015.

[20] 3GPP, Study on Scenarios and Requirements for Next Generation Access Technologies, 3rd Generation Partnership Project (3GPP), TR 38.913, Oct. 2016.

[21] A. Farhang, A. Aminjavaheri, N. Marchetti, L. E. Doyle, and B. Farhang-Boroujeny, Pilot decontamination in CMT-based massive MIMO networks, in 2014 11th International Symposium on Wireless Communications Systems (ISWCS). IEEE, 2014, pp. 589-593.

[22] A. Aminjavaheri, A. Farhang, L. Doyle, and B. Farhang-Boroujeny, Prototype filter design for FBMC in massive MIMO channels, in IEEE ICC 2017, May 2017.

[23] A. Aminjavaheri, A. Farhang, L. Doyle, and B. Farhang-Boroujeny," Filter Bank Multicarrier in Massive MIMO: Analysis and Channel Equalization," CS.IT 2017, 28 Jun 2017.

[24] A.Ijaz, et al.," Enabling massive IoT in 5G and beyond systems," PHY radio frame design considerations, IEEE Access, 2016, 3322-3339.

[25] 5GNOW deliverable D3.2 v1.3. 5G waveform candidate selection, 2014, Available at: $http://www.5gnow.eu$

[26] P.Xiao, C.Toal, D.Burns, V. Fusco and C.Cowan,"Transmit and receive filter design for OFDM based WLAN systems," International Conference Wireless Communications and Signal Processing (WCSP), October 2010, IEEE; pp. 1-4.

[27] E.Bala, J.Li and R.Yang, "Shaping spectral leakage: a novel low-complexity transceiver architecture for cognitive radio," IEEE Vehicular Technology Magazine, 2013,8(3),38-46.

[28] P. Siohan, C. Siclet, and N. Lacaille, Analysis and design of OFDM/OQAM systems based on filterbank theory , Signal Processing, IEEE Transactions on, vol. 50, no. 5, pp. 1170 - 1183, may 2002.

[29] A.Farhang, N. Marchetti and L.Doyle, Low complexity transceiver design for GFDM (forthcoming). arXiv:1501.02940.

[30] 5G: a technology vision, Huawei Technologies Co., Ltd., 2013. Available at: $https://www.scribd.com/document/251024709/5G-a-Technology-Vision$

[31] J.Du, P.Xiao, J.Wu and Q. Che, "Design of isotropic orthogonal transform algorithm-based multicarrier systems with blind channel estimation," IET Communications, 2012;6 (16):2695-2704.

[32] M.J.Abdoli, M.Jia, J.Ma, "Weighted circularly convolved filtering in OFDM/OQAM," IEEE 24th Annual International Symposium on Personal, Indoor, and Mobile Radio Communications (PIMRC), 8 September, 2013. pp. 657-661.

[33] B. Saltzberg, Performance of an Efficient Parallel Data Transmission System, Communication Technology, IEEE Transactions on, vol. 15, no. 6, pp. 805 - 811, december 1967.

[34] A. Viholainen, M. Bellanger, and M. Huchard. Prototype filter and structure optimization. website: www.ict-phydyas.org: Document D5.1 deliverable, Jan. 2009.

[35] J. Alhava and M. Renfors, Exponentially-modulated filter bank-based transmultiplexer, in Proc. IEEE Int. Symp. Circuits and Systems, vol. IV, pp. 233-236, May 2003.

[36] H. S. Malvar, Signal Processing with Lapped Transforms. Artech House, Boston, MA, USA, 1992.

[37] P. P. Vaidyanathan, Multirate Systems and Filter Banks. Prentice Hall, Englewood Cliffs, NJ, USA, 1993.

[38] M. Bellanger and J. Daguet, TDM-FDM Transmultiplexer: Digital Polyphase and FFT, Communications, IEEE Transactions on, vol. 22, no. 9, pp. 1199 - 1205, sep 1974.

[39] B. Hirosaki, An Orthogonally Multiplexed QAM System Using the Discrete Fourier Transform, Communications, IEEE Transactions on, vol. 29, no. 7, pp. 982 - 989, jul 1981.

[40] M.G. Bellanger, "Specification and design of prototype filter for filter bank based multi-carrier transmission," IEEE International Conference on Acoustic, Speech and Signal Processing, vol. 4, pp. 2417 - 2420 , May 2001.

[41] A. Viholainen, T. Ihalainen, T. Hidalgo Stitz, M. Renfors, and M. Bellanger, Prototype filter design for filter bank based multicarrier transmission, in 17th European Signal Processing Conference (EUSIPCO 2009), August 2009, pp. 1359-1363.

[42] T.A. Weiss and F.K. Jondral, Spectrum pooling: an innovative strategy for the enhancement of spectrum efficiency, Communications Magazine, IEEE, vol. 42, no. 3, pp. S8 - 14, mar 2004.

[43] C Ll, R Legouable and P Siohan; "Channel estimation with scattered pilots in OFDM/OQAM," In IEEE workshop on signal processing advances in wireless communications (SPAWC); 2008.

[44] C Ll, JG Javaudin, R Legouable , A Skrzypczak, P Siohan; "Channel estimation methods for preamble-based OFDM/OQAM modulations," Eur Trans Telecommun 2007;19(7),741-750.

[45] Du J, and Signell S. Novel preamble-based channel estimation for OFDM/OQAM systems. In: IEEE international conference on communication; 2009.

[46] S. Hu, G Wu, and S. Li, "Preamble design and iterative channel estimation for OFDM/offset QAM system," J Netw 2009;4(10):963-972.

[47] D. Katselis, E. Kofidis, A. Rontogiannis , S. Theodoridis, Preamble-based channel estimation for CP-OFDM and OFDM/OQAM systems: a comparative study. IEEE Trans Signal Process 2010;58(5):29116.

[48] [21] D. Katselis, M. Bengtsson,CR. Rojasa, H. Hjalmarsson, E. Kofidis, On preamble-based channel estimation in OFDM/OQAM systems. In: European signal processing conference; 2011.

[49] H. Lin and P.Siohan, Robust channel estimation for OFDM/OQAM. IEEE Commun Lett 2009;13(10):7246.

[50] E. Kofidis, D. Katselis, A. Rontogiannis, S. Theodoridi, Preamble-based channel estimation in OFDM/OQAM systems: a review. Signal Process 2013;93(7):203854.

[51] G. Garbo ,S. Mangione , V. Maniscalco, MUSIC-LS modal channel estimation for an OFDM-OQAM system. In: IEEE international conference on signal processing and communication systems (ICSPCS); 2008.

[52] LG. Haltar, M. Newinger, JA. Nossek, Structured subchannel impulse response estimation for filter bank based multicarrier systems. In: International symposium on wireless communication systems (ISWCS); 2012.

[53] D. Kong, D. Qu , T. Jiang, Time domain channel estimation for OQAM-OFDM systems: algorithms and performance bounds. IEEE Trans Signal Process 2014;63(2):32230.

[54] H.G. Feichtinger and T. Strohmer, Gabor analysis and algorithms: theory and applications, Applied and numerical harmonic analysis. Birkhuser, 1998.

[55] R. W. Chang, High-speed multichannel data transmission with bandlimited orthogonal signals, Bell Syst. Tech. J., vol. 45, pp. 1775 - 1796, Dec. 1966.

[56] G. Cherubini, E. Eleftheriou, and S. Olcer, Filtered multitone modulation for VDSL, in Global Telecommunications Conference, GLOBECOM 99, 1999, vol. 2, pp. 1139 - 1144.

[57] Crislin L*élé*, OFDM/OQAM : M*é*thodes $d^{'}$Estimation de Canal, et Combinaison avec $l^{'}$ Accès Multiple CDMA ou les Systèmes Multi-Antennes, Ph.D. thesis, Conservatoire National des Arts et M*é*tiers, Paris, France, 2008.

[58] V. Wong, R. Schober, D. W. K. Ng, L. W, 2017. Key Technologies for 5G Wireless Systems. 1st ed. United Kingdom: Cambridge.

[59] Qualcomm. 2016. Leading the World to 5G. [ONLINE] Available at: https://www.qualcomm.com/media/documents/files/whitepaper-5g-vision-for-the-next-generation-of-connectivity.pdf. [Accessed 3 May 2017].

[60] G. Fodor et al., "An Overview of Device-to-Device Communications Technology Components in METIS," in IEEE Access, vol. 4, no. , pp. 3288-3299, 2016.

[61] E. Eraslan and B. Daneshrad, "Low-Complexity Link Adaptation for Energy Efficiency Maximization in MIMO-OFDM Systems," in IEEE Transactions on Wireless Communications, vol. 16, no. 8, pp. 5102-5114, Aug. 2017.

[62] H. Q. Ngo, E. G. Larsson, and T. L. Marzetta, Energy and spectral efficiency of very large multiuser MIMO systems, IEEE Transactions on Communications, vol. 61, no. 4, pp. 1436-1449, 2013.

[63] A. M. Mathai and S. B. Provost, Quadratic forms in random variables: theory and applications. M. Dekker New York, 1992.

[64] Du Jinfeng and S. Signell, Comparison of CP-OFDM and OFDM/OQAM in doubly dispersive channels, in Future Generation Communication and Networking (FGCN 2007), Dec 2007, vol. 2, pp. 207211.

[65] C.Daniel, Arajo, Taras Maksymyuk, Andr L. F. de Almeida1, Tarcisio Maciel1, Joo C. M. Mota1, and Minho Jo; "Massive MIMO: Survey and Future Research Topics" , Evolution and the Revolution of 5G Wireless Communication Systems, Oct. 2016,